



## รายงานวิจัยฉบับสมบูรณ์

# โครงการ: สมบัติเชิงโครงสร้างและอิเล็กตรอนของ สารประกอบกลุ่ม III-V ที่ผ่านการโดปภายใต้ สภาวะรุนแรง

โดย ผู้ช่วยศาสตราจารย์ ดร.ประยูรศักดิ์ เปลื้องผล

เดือน ปี ที่เสร็จโครงการ มิถุนายน พ. ศ. 2560

## สัญญาเลขที่ TRG5880006

## รายงานวิจัยฉบับสมบูรณ์

โครงการ: สมบัติเชิงโครงสร้างและอิเล็กตรอนของ สารประกอบกลุ่ม III-V ที่ผ่านการโดปภายใต้ สภาวะรุนแรง

ผู้ช่วยศาสตราจารย์ ดร.ประยูรศักดิ์ เปลื้องผล มหาวิยาลัยหัวเฉียวเฉลิมพระเกียติ

สนับสนุนโดยสำนักงานกองทุนสนับสนุนการวิจัย และต้นสังกัดมหาวิทยาลัยหัวเฉียวเฉลิมพระเกียติ

(ความเห็นในรายงานนี้เป็นของผู้วิจัย สกว.และต้นสังกัดไม่จำเป็นต้องเห็นด้วยเสมอไป)

## บทคัดย่อ

รหัสโครงการ: TRG5880006

ชื่อโครงการ: สมบัติเชิงโครงสร้างและอิเล็กตรอนของสารประกอบกลุ่ม III-V ที่ผ่านการ

โดปภายใต้สภาวะรุนแรง

ชื่อหักวิจัย: ผู้ช่วยศาสตราจารย์ ดร.ประยูรศักดิ์ เปลื้องผล

มหาวิยาลัยหัวเฉียวเฉลิมพระเกียติ

ที่อยู่อีเมลล์ : prayoonsak@gmail.com

ระยะเวลาโครงการ : 2 ปี

โครงสร้างและสมบัติเชิงอิเล็กตรอนของสารประกอบกลุ่มIII-Vที่ผ่านการโดปภายใต้ สภาวะรุนแรงได้ทำการศึกษา สมบัติเชิงโครงสร้าง สมบัติเชิงอิเล็กตรอน สมบัติทางแสง และ สมบัติทางกล โดยการแทนที่อะตอมของสังกะสี (Zn) ซิลิกอน (Si) ดีบุก (Sn) และกำมะถัน (S) ลงในโครงสร้างอินเดียมฟอสไฟด์ในโครงสร้างซิงค์เบลน (ZB) และแบบหินเกลือ (RS) ได้รับการ ดีพิมพ์ในวารสารระดับนานาชาติ ผลวิจัยพบว่ากระบวนการแทนที่เกิดได้ดีในโครงสร้างแบบหิน เกลือมากกว่าในซิงค์เบลน พันธะเคมี Zn-P ในซิงค์เบลนแข็งแรงที่สุดเมื่อเทียบกับชนิดอื่นๆ ซึ่ง คือ Zn-P>Si-In>S-In>Sn-In ตามลำดับ ความเป็นไดอิเล็กตริกของสารอินเดียมฟอสไฟด์ลดลง เมื่อสารถูกโดปและกลายเป็นโลหะที่ความถี่สูง ลำดับของสัมประสิทธิ์การดูดกลืนแสงเทียบกับ สารเจือ คือ Sn>Si>S>Zn และมันลดลงภายใต้ความดันที่สูงขึ้น ความเสถียรทางกลได้รับการ ทดสอบและเป็นไปตามหลักความเสถียรของบอร์น สารเจือลดมอดุลัสเฉือนของอินเดียมฟอส ไฟด์ อัตราส่วนมอดุลัสบ่งชี้ว่าความแข็งเหนียวของอัลลอยด์อินเดียมฟอสไฟด์ลดลงเมื่ออยู่ใน โครงสร้างแบบหินเกลือ และความแข็งเหนียวของสารจะลดลงได้เนื่องจากผลของการเจือให้ เป็นอัลลอยด์

คำหลัก: โครงสร้างเสถียร สมบัติความยืดหยุ่น อัลลอยด์กลุ่ม III-V ความดันสูง

#### **Abstract**

Project Code: TRG5880006

Project Title: Structural and electronic properties of doped III-V binary compounds

under extreme conditions

Investigator: Assistant Professor Dr. Prayoonsak Pluengphon

**Huachiew Chalermprakiet University** 

E-mail Address : prayoonsak@gmail.com

Project Period: 2 years

Structural and electronic properties of doped III-V binary compounds under extreme conditions were studied. Structural, electronic, optical and mechanical properties of Zn, Si, Sn and S substitutions on InP supercell under pressure in zinc blende (ZB) and rock salt (RS) phases were published on an international journal. It was found that the lower enthalpy difference in RS structure indicates that the spontaneous process of impurity substitution can be occurred in RS more than in ZB. The chemical bonding of Zn-P in ZB is the strongest sharing electrons when compared with other compounds, Zn-P>Si-In>S-In>Sn-In. The dielectric performance of InP is reduced by the alloying effect, and it transforms to the conductor performance as high frequencies. Order of photo-absorption coefficient in range of visible light with the impurities is Sn>Si>S>Zn, and it reduces under high-pressure. Mechanical stability of InP alloys was observed, and satisfied the Born stability criteria. The impurities reduce Shear modulus of pure InP. *B/G* ratio indicates that ductility of InP alloys is reduced, when it transformed to RS. The ductility of InP is induced by the alloying effect due to the *B/G* ratio increasing.

Keywords: Phase stability, Elastic properties, III-V alloys, High-pressure

## Content

Topic	Page
Chapter I Introduction	1
Chapter II Methodology	7
Chapter III Results and discussion	13
Chapter IV Conclusions	28
References	30
Appendix	32
Output	43

### Chapter I

#### Introduction

#### 1.1 Introduction to the research problem and its significance

Nowadays, the extreme conditions in physics which mainly consist of high pressure and high temperature conditions are the essential topics for studying the tendencies of condensed matter characteristics. The extreme conditions are widely studied in pure and applied sciences as follows. In food science, high-pressure in range of megapascal (MPa) to gigapascal (GPa) was applied for food preservation which is non-thermal processing. Biological hazard in food was inhibited by high-pressure. In geology and geophysics, the physical properties of Earth's materials under extremely high pressure and temperature conditions are the important knowledge for studying the mechanisms of materials in the inner and outer core of the Earth. When we knew the mechanism and physical properties of Earth's materials under the extreme conditions, it can be suggested to predict the natural phenomenon of the Earth, especially the effects on the Earth's surface such as earthquake and tsunami. In physics and chemistry, the major topics about extreme conditions are focused on both physical and chemical properties such as physical hardness, bulk modulus, structural phase transitions, electronic structures, chemical reactions, optical properties and etc. These indicate that high-pressure and temperature effects are the significant parameters for applying to change the material properties. Therefore, the effects of extreme conditions on the interesting materials are mainly focused in this research.

Semiconductor materials especially III-V binary compounds are widely used in the applications devices which mainly depend on the electronic properties such as transistors, solar cells, light-emitting diodes, integrated circuits and etc. The electrical conductivity of semiconductor depends on the temperature and pressure effects. It increases when temperature increasing which opposite with metal. The electrical properties of semiconductor can be modified by adding impurities. The conductivity of semiconductor occurs due to the movement of carriers which are electron in conduction band (e) and hole in valence band (h). Adding the impurities atom on intrinsic semiconductor, which called doped semiconductor, can change the charge carriers and ratio of electron and hole. Type of doped semiconductor including n-type (e>h) and p-

type (h>e) was defined by the ratio of electron and hole concentrations. In this work, we would like to change charge carriers by adding the doping on III-V binary compounds.

In the experimental and theoretical studies under extreme conditions, the highpressure conditions of the condensed materials were adopted by using diamond anvil cell (DAC) to press the high pressure on a material. DAC consists of two opposing diamonds with a sample compressed between the culets. The pressure compressing from DAC device can be generated in order of GPa. The stability of structures and some physical properties of a material under high pressure can be obtained from studying X-ray diffraction pattern. However, the maximum of high pressure which is produced from DAC device has a limit. The theoretical simulation is a suitable method to access the hidden conditions from experiments. The complicated properties from experiments can be compared and extended by using theoretical simulations such as ab initio approach. Ab initio method is one of popular techniques to solve the properties of condensed matter. In physics and chemistry, density functional theory (DFT) is the most popular and successful theory for solving the solution in many-body problems. It was used to suggest the phase transitions and physical properties in solid periodic system. For studying the thermal effect in DFT calculation, temperature will be added in the molecular dynamics (MD) calculation. The frozen structures in 0 K will be relaxed by the lattice vibration in molecular dynamics. The advantages of simulation methods are giving predictions, extending experimental results, and proving theories from principle conceptions.

In this work, we would like to study the structural and electronic properties of doped III-V binary compounds under extreme conditions. The high-pressure and temperature effects are interested in this work because these effects are the significant parameters for changing material properties. We interested in the III-V binary compounds because it was widely used in application devices. The charge carriers in intrinsic semiconductors can be changed by adding the doping effect on the host semiconductors. Therefore, the doping effect is the significant figure in this work. We think that DFT calculation can give the details of physics concept for explaining physical properties of the undoped and doped III-V binary compounds. The physical properties of the interesting semiconductors such as crystal structures, phase transitions, electronic density of states, band structures and photo-absorption coefficients will be investigated in this research. Moreover, we would like to compare the calculation result with the experiments. The sample materials will be added high-pressure condition by using DAC instrument. Physical properties will be observed by using XRD and other

measurements. For the advantages from this work, we expect that the fundamental data about the exact properties under extreme conditions of undoped and doped III-V compounds from this work can suggest the suitable conditions for application devices. Therefore, we believe that the novel information will be obtained from the extreme conditions research in this work.

#### 1.2 Literature review

At ambient pressure, the binary compound semiconductors in the group of III-V were widely used in many applications such as solar cell fabrications and diode devices. In previous works of our team in Extreme Conditions Physics Laboratory, Department of Physics, Faculty of Science, Chulalongkorn University, we firstly studied high pressure properties of GaAs. The structural and mechanical properties of GaAs up to 200 GPa were reported in P. Pluengphon et. al. Solid State Communications, 195 26-30 (2014). The stability of GaAs structures was considered by comparing the minimum free energy or enthalpy of system. From observation by using LDA functional, we found that the high-pressure phases of GaAs are ZB (0-12 GPa), Cmcm (12-37 GPa), Imm2 (37-88 GPa), Pmma (88-146 GPa) and P4/nmm (146-200 GPa), respectively. The difference results from theoretical and experimental reports were concluded that Pmma and P4/nmm are the distorted structures of P6/mmm and CsCl-like, respectively. The lower symmetric phases gave the minimum free energies. Transformation path from Pmma to P4/nmm phases was estimated and found that P6/mmm changes to P4/nmm in direction [1 1 0]. The enthalpy barrier of this path is 0.035 eV. In addition, physical properties of the metallic phases GaAs were examined by analyzing the elastic parameters. The continuous of EDOSs show the metallization of Pmma and P4/nmm phases. The electron density difference contour plots show that the sharing electron in Pmma is higher than in P4/nmm. This indicates that Pmma has the characteristic of the covalent bond. From the modulus ratio, it can be concluded that Pmma phase is a ductile material, while the P4/nmm phase is a brittle. After GaAs high-pressure properties were studied, we would like to extend the high pressure studies to the semiconductors in III-V group. Moreover, we interested the previous studies about the doping in III-V binary compounds. Mn-doped Ga-V semiconductors are amongst the most interesting materials for applications in such new devices. Mn-doped on GaAs is called that a diluted magnetic semiconductor (DMS). The Curie temperature T<sub>c</sub> of (Ga,Mn)As linearly dependent on the concentration of the substitution Mn. The impurity of Mn exhibits the carrier-induced ferromagnetism which controlled by the carrier density. By molecular beam epitaxy (MBE), it was found that the Mn impurity increases the Curie temperature, lattice constant and impurity band. The most Mn atoms preferably substitute on cation sites of GaAs. Alberi et al. suggested that Mn increases the impurity band of GaAs which increases in strength with Mn concentration. The formation of the impurity band arises as the anticrossing interaction between the localized and extended p states of the Mn atoms and GaAs. By using tight-binding models, Turek et al. found that Mn increases the number of holes for low concentrations (x<0.02). For higher concentrations x, it exhibits qualitative changes including strong localization of eigenstates with energies close to the band edge. For Mn-doped GaN, J.J. Kim et al. observed that Mn doping introduces a new structure in the band gap region near the top of the valence band, and also a broader structure in deeper valence band region. Basing upon the first principle calculation, these structures are assigned as Ga 4s originated states, which are raised by hybridization between 3d orbitals of Mn with GaN host orbitals. M. Zajac et al. using x-ray diffraction showed characteristic diffraction lines for hexagonal GaN phase mixed with a small contribution (<5%) from the Mn<sub>3</sub>N<sub>2</sub> phase. Raman spectra exhibited characteristic peaks of pure GaN and modes that could be associated with Mn-induced lattice disorder.

Indium Phosphide (InP) is one of most promising materials in a III-V group which used as a substrate for epitaxial growth applied in photovoltaic multilayers [1-3]. InP is widely used in high-frequency and high-power electronic devices because it has superior electron velocities and long-lived optical phonons when compared with other III-V compounds [3, 4]. Stable crystal structure of InP at ambient pressure (0 GPa) is zinc blende (ZB) in space group F-43m [5-7], which related with most of III-V semiconductors such as GaAs, GaN, InAs and InSb. When high-pressure in order of gigapascal (GPa) presses on a primitive cell, the stable structure of InP has the transformations in each pressure range as F-43m-->Fm-3m-->Cmcm-->Immm-->Pm-3m at 5.6, 11.0, 50.0 and 102.0 GPa, respectively [7]. The 2<sup>nd</sup> phase of InP is rock salt (RS) phase in space group Fm-3m. The 1<sup>st</sup> transformation path from ambient phase to RS normally deforms to non-semiconductor due to the reconstruction bonding of disorder to order structures during phase transition that found in CuGaSe<sub>2</sub> [8,9] and GaAs [10,11]. High-pressure condition and structural phase transition have highly effected on chemical bond, band structure, electronic density of state (EDOS), photo absorption, elasticity and superconductivity [12-14]. Bouarissa studied high-pressure effects on the properties of InP, including electronic and optical properties [15], valence and conduction charge densities [16], and bonding and iconicity [17]. It was found that electronic charge densities are sensitive to the effect of hydrostatic pressure and the transverse effective charge decreases with increasing pressure which indicates the increased covalent bonding in the InP. In addition, the effects of impurity atoms on InP at ambient pressure have widely studied because the electronic and optical properties respond significantly with the concentration of impurities [18-23]. Zn-doped InP layers were obtained by in situ doping in low pressure metalorganic chemical vapor deposition, and thermal diffusion from a Zn-containing film [18]. Band edge peaks and band of shallow donor to acceptor transition peak were observed in in situ Zn-doped InP, implying that interstitial Zn atoms were generated during in situ doping. Schubert et al. [19] reported that Zn diffusion depends strongly on the concentration of Zn. Zn-doped is preferable in InP over other p-type dopants because it has high electrical activity, moderate diffusion, controllable incorporation and low residual toxicity. And then, the incorporation and doping process of Si, S and Zn impurities in InP by metalorganic vapor phase epitaxy have been studied both standard growth conditions and selective area growth conditions [20]. It was found that Zn-S co-doping shows a Zn dopant concentration enhancement in selective area growth conditions, while it remains constant in standard growth conditions. The Si concentration was unexpectedly independent of the growth rate in selective area growth conditions. Youssef [21] studied optical properties of Zn-doped InP, and found that Zn-doped increases refractive index and reduces band gap of InP.

From the literature review, we can see that the gap of previous studies is incomplete of high-pressure properties which will be investigated in this research. In this work, the III-V binary compounds are mainly interested because it is widely used in photovoltaic materials in solar cell. The effects of pressure and temperature are mainly point to improve the suitable properties for solar cell applications. In addition, the doping effect is an important role for changing the electronic properties in semiconductors. At the beginning of methodology, GaAs and InP are the interested materials in this work. Stable structures of InP under pressure are mainly fundamental data to verify our calculation. The attractive point of this work is the high-pressure properties of doped III-V semiconductors with varying temperature of system, because the previous publications widely studied the doping semiconductors only at ambient pressure (0 GPa) but under high-pressure are still incomplete. We will observe the crystal structures, phase transitions, electronic density of states, band structures and photo-absorption coefficients. We think that our framework differs from previous researches. Fundamental knowledge of the high-pressure properties of doped GaAs, InP and other III-V

compounds will be carried out. It is strongly believed that the novel information in this work will be published to the international journals, and suggested to fabricate such application devices.

### 1.3 Objectives

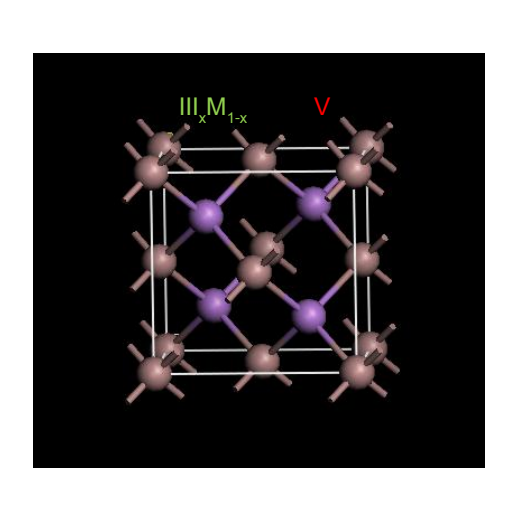
- To understand the structural phase transitions of undoped and doped III-V binary compounds.
- To understand the electronic properties, including crystal structures, electronic density of states, band structures and photo-absorption coefficients, of doped III-V binary compounds under extreme conditions.
- 3. To obtain novel information from this work.
- 4. To publish the novel information in the international publications.

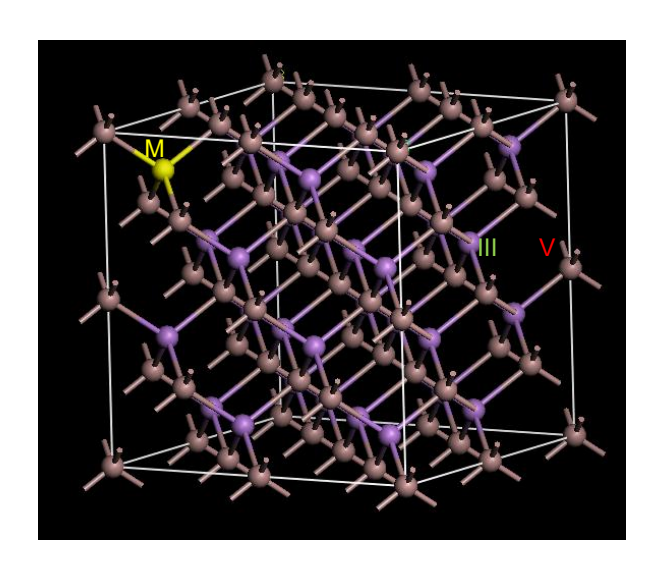
## **Chapter II**

## Methodology

In this work, an ab initio or first-principle method is mainly used for finding the structural phase transitions and the electronic properties, including electronic density of states, band structures and photo-absorption coefficients, of doped III-V binary compounds under extreme conditions. And then, the calculation result will be compared with the experimental measurements of sample materials obtained from DAC. The ab initio method by using CASTEP (Cambridge Serial Total Energy Package) code is a software package which uses density functional theory (DFT) with a plane wave basis set to calculate the electronic properties of crystalline solids, surfaces, molecules, liquids and amorphous materials from first principles. The properties of bulk materials can be obtained from solving the basic laws in a unit cell. In DFT, the ground states properties such as density of electrons and total energy are evaluated by solving Kohn-Sham equations and self-consistent field method (SCF). Ab initio studies were generated from basic laws in atomic scale or particle level, and calculated without using the results from experiments. Ab initio calculation with DFT is a theoretical method which started from the basic laws in many-body system but the practical process has used some approximations for generating the exchange-correlation functional. The first successful result from solving Kohn-Sham equations is total energy of ground state system. The crystal structures and physical properties of a bulk material were determined by changing the thermodynamics states such as changing temperature or pressure. The outcome of ground state properties of a solid system can be calculated by solving Kohn-Sham equations. Kohn-Sham equations are Schrodinger-like equations of one particle in effective potentials of a many-body system. However, Kohn-Sham equations obtained from Hohenberg-Kohn theorems which interested in non-degenerate ground state system. All ground state properties are the functional of electron density in a system. As a result, Eigenfunction obtained from the eigenvalue problem of Kohn-Sham equations is not wavefunction of electron but it called Kohn-Sham orbitals which have no physical meaning. Eigenvalue can be linked to total energy of system under given volume of unit cell. The solutions of ground state properties from Kohn-Sham equations highly depend on type of the exchange-correlation functional contained in the effective potential of system. The powerful exchange-correlation functional for all material is still

not found. The first investigation in DFT simulation work is to find the suitable exchange-correlation functional for predicting the interested properties. understanding about the DFT, we firstly observed phase transition prediction as shown in the last publication (P. Pluengphon et. al. Solid State Communications, 195 26-30 (2014)). GaAs high pressure phases in Durandurdu and Drabold's work were extended up to 200 GPa. The simple hexagonal phase from the experiment was verified by using CASTEP calculation. Types of GaAs high-pressure phases, such as semiconductor, semimetal and metal, were classified by studying the electronic density of state (EDOS). Moreover, the elastic constants, bulk modulus, Young's modulus and shear modulus will be observed at very high pressure also.





(a) VCA method

(b) Super cell method

**Figure 2.1** (a) M was mixed in all III-A atoms ( $III_xM_{1-x}$ ) the potential of mixed atoms were generated by using virtual crystal approximation. (b) Super cell was generated and Mn was substituted on III-A site.

After the high-pressure phases of pure III-V were studied, the M doped on III-V will be studied. We have two types of models for adding the M impurity atom on III-V that are virtual crystal approximation (VCA) and super cell methods as shown in figure 2.1. In figure 2.1(a), M was mixed in all III-A atoms ( $III_xM_{1-x}$ ) the potential of mixed atoms were generated by using virtual crystal approximation. We have reported the VCA method in  $Cu(In,Ga)Se_2$  and found that the mixing potential gave a good result at low concentration of impurity (x < 0.1). Therefore, the impurity in this work will be studied in the range of x = 0-0.1. In figure 2.1(b), super cell of III-V was generated, and M was

substituted on a III-A site. We have the experience about doped III-V compound. The first impurity atom in this work is Mn atom because the effects of Mn on GaAs-ZB at ambient pressure are widely studied much more. However, the effect of Mn under high pressure is not complete. The results from 2 methods are compared and extended from the experiment at ambient pressure. High pressure effect added in periodic system by reducing volume cell. Super cells consist of host and impurity atoms will be relaxed by geometry optimization. Temperature effect can be studied by molecular dynamics. Moreover, it was well known that the impurities in semiconductors are not periodic systems. The interaction between 2 impurity atoms in a super cell will be studied as shown in figure 2.2. The distance between 2 impurity atoms will be varied in a super cell.

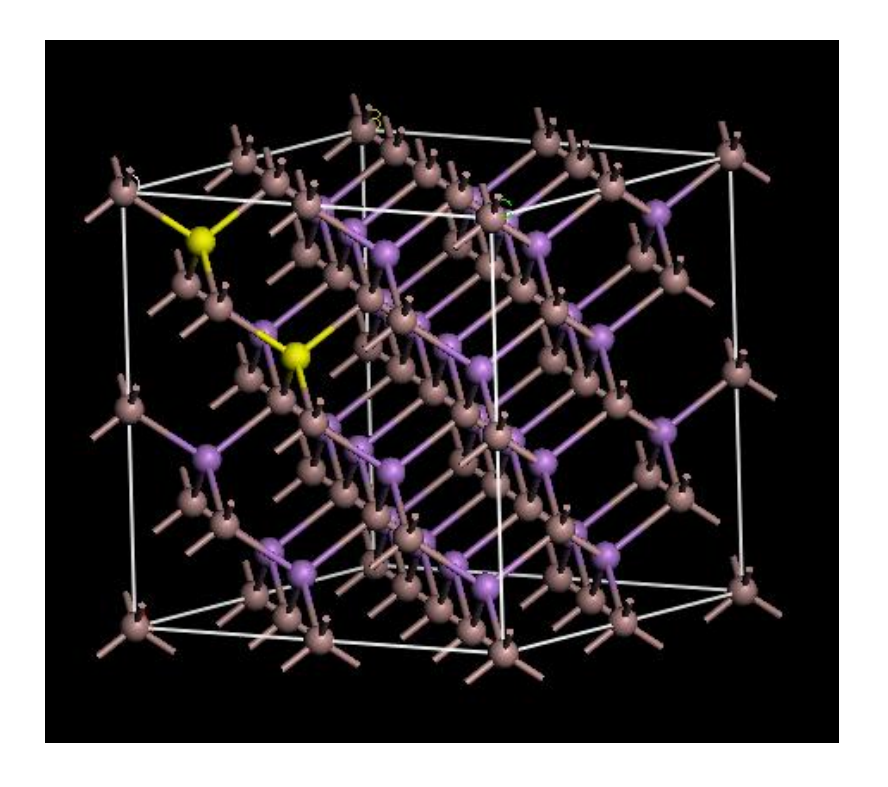


**Figure 2.2.** Structure of doped III-V for study the interaction between 2 impurity atoms in super cell.

The effects of impurity on the band structure, EDOS and photoabsorption of GaAs and other III-V compounds under high pressure phases will be analyzed. For example, we have firstly investigated the primary results of the  $Ga_{1-x}Mn_xAs$  structures. For generating the  $Ga_{1-x}Mn_xAs$  structures, the Mn atom was substituted on a Ga site in GaAs super cells.  $Ga_{1-x}Mn_xAs$  structures were varied at x = 0.037, 0.083 and 0.125 which obtained from substitution of Mn atom on a Ga site in the GaAs super cells sizes  $2 \times 2 \times 2$ ,  $2 \times 2 \times 3$ 

and 3×3×3, respectively. For example, super cell size 2×2×2 of GaAs in ZB was substituted by a Mn atom at a Ga site which called Ga<sub>0.963</sub>Mn<sub>0.037</sub>As as shown in figure 1(b). The optimum cutoff energies for getting the total energy convergences of Ga<sub>1-</sub> "Mn, As in super cells 2×2×2, 2×2×3 and 3×3×3 were found at 350 eV for the calculations of geometry optimizations, single point energies, electronic and optical properties. Forces on the optimized atomic positions were calculated by using the Hellmann-Feynman theorem. We have observed phase transition from ZB to Cmcm and found that phase transition from semiconductor (ZB) to nonsemiconductor (Cmcm) phase from our calculation occurred at 12 GPa, therefore; we selected to calculate the properties of (Ga,Mn)As at the pressure 0, 5 and 10 GPa. After we optimized the doped super cells, the EDOS and absorption coefficient of Ga<sub>1-x</sub>Mn<sub>x</sub>As were calculated by using the generalized-gradient approximation functional of Perdew-Burke-Ernzerhof (GGA-PBE). The condition in each direction of k-point sampling of Monkhorst-Pack grid size is  $1/k \le 0.05$  for calculations the properties of super cells. After we obtained the stable structures from the geometry optimizations, photoabsorption coefficient can be calculated from the imaginary part of complex refractive index which relate with the complex dielectric function ( $\varepsilon = \varepsilon_1 + i \varepsilon_2$ ). The real ( $\varepsilon_1$ ) and imaginary parts ( $\varepsilon_2$ ) of dielectric function that evaluated from the matrix elements of the position operator are required to describe the electronic transitions. Photoabsorption coefficient is calculated by using Eq. (2.1)

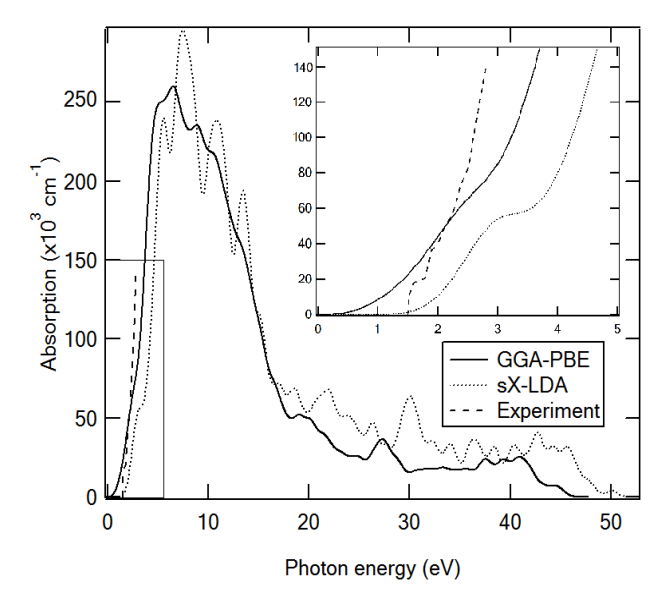


**Figure 2.3** Comparisons the absorption coefficients of GaAs at 0 GPa from the GGA-PBE, sX-LDA calculations and the experiment result with photon energy 0.6-2.75 eV at 21 K.

$$I(\omega) = 2\omega \left( \frac{\sqrt{\varepsilon_1^2(\omega) + \varepsilon_2^2(\omega)} - \varepsilon_1(\omega)}{2} \right)^{1/2}$$
 (2.1)

Photoabsorption coefficient indicates the fraction of energy lost by the wave when it passes through the material. For optical band gap discussion, it is well known that GGA-PBE functional gave the wrong band gap in semiconductor. The photoabsorption coefficient calculated from the GGA-PBE functional was compared with the screened exchange local-density approximation (sX-LDA) functional as shown in figure 2.3.

In during 2 years for study this research, these models will be used in other doped III-V compounds. The temperature effect and vibration of doped lattices will be observed in (Ga,Mn)As, (In,M)P, In(M,P) and other compounds. The interaction between two impurity atoms in a super cell will be carried out. For the main expectance of this work, we believed that it differs from previous researches, especially understanding the tendencies of high pressure properties of doped GaAs and other III-V compounds. It is strongly believed that the novel information from this work can give the attractive knowledge of III-V compounds for application devices. In this work, the results from ab initio calculation will be compared with the experiments. The III-V binary compounds will be pressed by using diamond anvil cell (DAC). In this work, the doped III-V compounds under extreme conditions are observed by theoretical and experimental investigations. In theoretical method, the ab initio method is mainly used for finding the structural phase transitions and the electronic properties, including electronic density of states, band structures and photo-absorption coefficients, of doped III-V binary compounds under extreme conditions. The ab initio method is based on the density functional theory (DFT). The properties of bulk materials can be obtained from solving the basic laws in a unit cell. In DFT, the ground states properties such as density of electrons and total energy are evaluated by solving Kohn-Sham equations and self-consistent field method (SCF). We have two types of models for adding the Mn impurity atom on GaAs that are virtual crystal approximation (VCA) and super cell methods. In experimental investigations, the doped sample materials are prepared in furnace and other devices at Department of Physics, Faculty of Science, Chulalongkorn University. A furnace is a device used for high-temperature heating. The impurity of atom in III-V compound is varied by weight. And then, high pressure conditions in doped compounds can be added by DAC. Crystal structures of doped III-V compounds are observed by XRD. The temperature effects and vibration modes of doped lattices will be observed by molecular

dynamics. The interaction between two impurity atoms in a super cell will be carried out. The results from ab initio calculation will be compared with the experiments. The doped samples will be prepared in furnace and other devices. The high-pressure on doped compounds will be observed by DAC. And then, physical properties can be observed by XRD and other devices. For the main expectance of this work, we believed that it differs from previous researches, especially understanding the tendencies of high pressure properties of doped GaAs and other III-V compounds. It is strongly believed that the novel information from this work can give the attractive knowledge of III-V compounds for application devices.

## **Chapter III**

#### **Results and discussion**

High-pressure properties of the doped III-V compounds are investigated. To study the DFT calculations in the undoped and doped InP systems as shown in figure 3.1, the local density approximation schemes of Ceperley-Alder-Perdew-Zunger (LDA-CAPZ) and the generalized-gradient approximation functional of Perdew-Burke-Ernzerhof (GGA-PBE) [23, 24] are compared at ambient condition for finding the suitable exchange-correlation functional term in Kohn-Sham equations. In table 3.1, it was found that the lattice parameters and bulk modulus of InP calculated from LDA-CAPZ functional are better than GGA-PBE results; therefore, LDA-CAPZ is mainly used as exchange-correlation functional for finding the high-pressure properties of the undoped and doped InP systems. This supported the DFT results in ZB structure of GaAs (III-V) semiconductor in previous work [11].

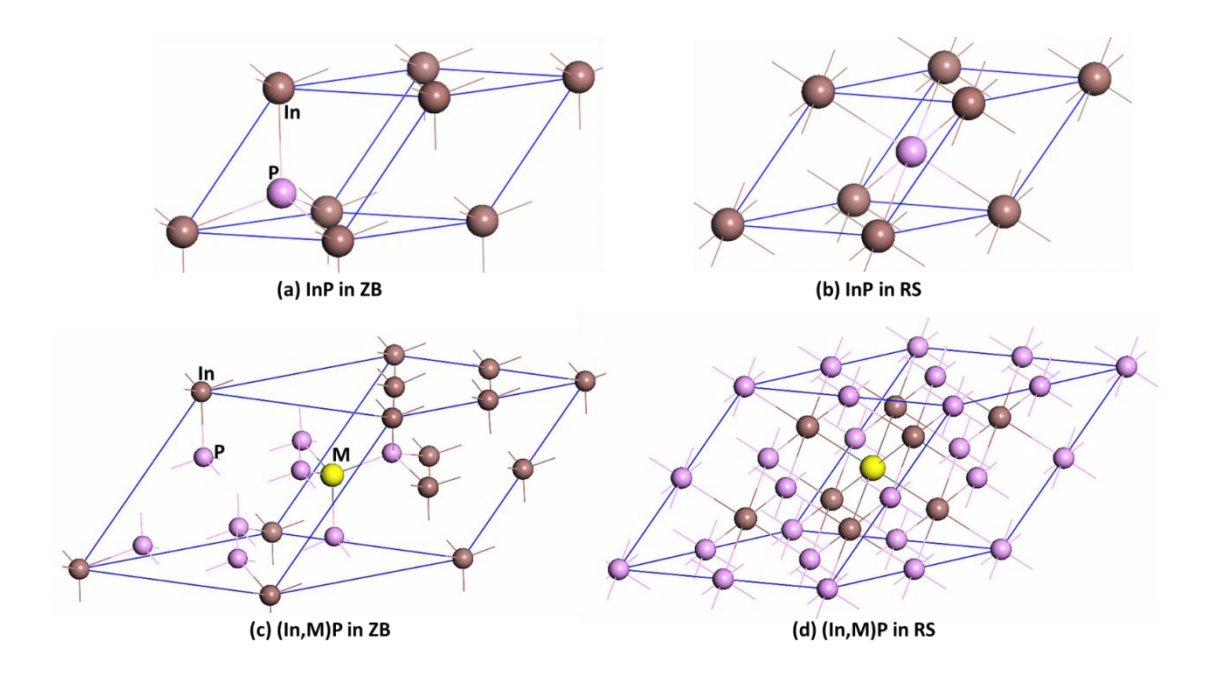


Figure 3.1: Atomic structures of InP in pure and alloys conditions (a) InP in ZB structure (b) InP in RS structure (c) InP replaced by M atom in ZB supercell (d) InP replaced by M atom in RS supercell.

Table 3.1: Lattice parameters (a=b=c), volume cell (V) and bulk modulus ( $B_0$ ) at 0 GPa in ZB structure of InP compared with previous studies [3, 6].

a (Å)	<i>V</i> (Å <sup>3</sup> )	<i>В</i> <sub>0</sub> (GPa)	Method	Ref.
5.968	212.6	59.3	GGA-PBE	This work
5.832	198.4	71.8	LDA-CAPZ	This work
5.869	202.2	71.0	EPM	[3]
5.856	200.8	71.1	Experiment	[6]

To study the doped InP, the impurity atoms which consist of Zn, Si, Sn and S are substituted on In (or P) site in 1/8 of InP with super cell size 2×2×2. The maximum energy of plane wave basis set used at 450 eV, which is suitable cutoff energy to cooperate with ultrasoft-pseudopotential [25]. Monkhorst-Pack grid sizes [26] for 2×2×2 super cells both ZB and RS structures are 8×8×8, while k point in undoped InP initially finites as the condition of k=0.03. The Brodyden-Fletcher-Goldfarb-Shanno (BFGS) [27] minimization scheme is used in geometry optimization. External forces and pressure tensors on optimized structures are controlled by Hellmann-Feynman theorem [28]. The BFGS optimization was considered to be completed when the total energy difference was less than 2×10<sup>-6</sup> eV/atom, Hellman–Feynman forces were less than 0.006 eV/Å, the maximum ionic displacement within 0.0002 Å, and all of the stress components within 0.003 GPa. The average isotropic modulus in bulk obtained from elastic constants by Voigt-Reuss-Hill (VRH) method [29, 30].

#### 3.1 Site preference and phase stability

Formation enthalpy and free energy difference at 0 GPa are analyzed as shown in table 1. Formation enthalpy per atom ( $H_f$ ) of  $In_{1-x}M_xP$  (or  $M_{ln}$ ) compound can calculate in form [31]

$$H_{f} = \frac{1}{2} H_{total} \left( \operatorname{In}_{1-x} M_{x} P \right) - \frac{1}{2} \left[ \left( 1 - x \right) H_{solid} \left( \operatorname{In} \right) + \left( x \right) H_{solid} \left( M \right) + H_{solid} \left( P \right) \right]$$

where  $H_{total}$  is the enthalpy of  $In_{1-x}M_xP$  compound, and  $H_{solid}$  is the enthalpy of In, M and P in the solid form. Formation enthalpy is used to compare the change of enthalpy during the formation of the  $In_{1-x}M_xP$  compound from its constituent elements, while

stability and possibility of process to occur a doped compound can considerate from free energy difference:

$$\Delta G = G - G_0 = H - H_0$$
 at 0 K

where G and  $G_o$  are Gibbs's free energies of doped and undoped conditions at a given pressure.

Table 3.2: Formation enthalpy and free energy difference of doped and undoped InP at ambient pressure 0 GPa.

ambient pressure o Gra.							
compound	$H_{ extit{total}}$	$H_{f}$	G-G <sub>0</sub>				
InP	-870.40	-4.29	0.00				
Zn <sub>In</sub>	-879.66	-4.16	-9.26				
S <sub>P</sub>	-876.51	-4.17	-6.12				
Si <sub>In</sub>	-779.47	-4.36	90.93				
Si <sub>P</sub>	-865.76	-4.16	4.64				
Sn <sub>In</sub>	-778.73	-4.27	91.67				
Sn <sub>P</sub>	-865.02	-4.07	5.38				

The enthalpy per atom of InP at 0 GPa in table 3.2 is  $H_0$  = -870.40 eV, using as the base line of free energy for comparisons. Site preference of Zn (II-B group) impurity is the substitution on the In site with  $H_f$  = -4.29 eV, while S (VI-A group) atom prefers to substitute on P site with  $H_f$  = -4.17 eV. These depend on position of elements and electronegativity values in periodic table. Zn-doped result supported the p-type Zn doping in InP [15, 16]. Zn is donor atom in the host InP semiconductor, while S is acceptor atom. We also observe the substitution of impurities in IV-A group (Si and Sn). The formation enthalpies when Si or Sn substituted on In site (Si<sub>In</sub> and Sn<sub>In</sub>) are lower than on P site equal to 0.2 eV/atom. It is possible that In site is a preference site of the Si and Sn doping. However, we found that a free energy of InP system highly increases when it was substituted in the forms Si<sub>In</sub> and Sn<sub>In</sub> as 90.93 eV and 91.67 eV, respectively. On the other hand, it reduces in the forms of Si<sub>P</sub> (4.64 eV) and Sn<sub>P</sub> (5.38 eV). It was found only Zn<sub>In</sub> and S<sub>P</sub> that gave both  $H_f$  and  $\Delta G$  < 0. Zn on In site (Zn<sub>In</sub>)

gives the minimum free energy difference as  $\Delta G = -9.26 \; \mathrm{eV}$ . Therefore, it is possible that Zn and P can substitute on InP without the external stimulations.

Table 3.3: Free energy difference of InP alloys in ZB and RS under pressure.

Structure	P (GPa)	G <sub>o</sub>	G- G <sub>o</sub>			
		InP	Zn <sub>In</sub>	Si <sub>P</sub>	Sn <sub>P</sub>	S <sub>P</sub>
ZB	0	-870.40	-9.26	4.64	5.38	-6.12
	5	-869.60	-9.29	4.64	5.41	-6.10
	10	-868.84	-9.31	4.65	5.43	-6.09
RS	5	-869.42	-9.37	3.09	3.74	-6.28
	10	-868.80	-9.39	3.05	3.72	-6.28

To compare the ZB and RS phases, we observed free energies and the enthalpy-pressure (H-P) curve between two phases. The calculated phase transition occurred at 12 GPa that are in consistent with previous works [1, 7]. We knew that the doping effect on semiconductor has small effect on the transition pressure [32]. Therefore, the properties of doped compounds in ZB and RS will be compared at 5 and 10 GPa which near the transition pressure from ZB to RS. At the high-pressure 5 and 10 GPa in table 3, we found that high-pressure has small effect on  $\Delta G$ , while the influence of phase transition ZB-RS is larger than. As the same pressure, a free energy difference of all compounds in RS is lower than in ZB. This indicates that the substitutions of Zn, S, Si, Sn impurities in the RS structure are easier than in the ZB.

### 3.2 Electronic properties

The electronic properties of Zn, S, Sn and S doped InP in ZB and RS phases are analyzed. It was found that the EDOSs in ZB structure at 0, 5 and 10 GPa show band gap between valence band and conduction band, which the Fermi level set at the energy 0 eV. Band gap vanished in RS structure both 5 and 10 GPa. Therefore, the semiconductor in ZB changes to non-semiconductor in RS due to the closing of band gap as shown in figure 3.2(a). The 1<sup>st</sup> phase transition (ZB-RS) has highly effected on

the electronic structure. In figure 3.2(b), the doping of Si and Sn reduce band gap of InP, and generate the impurity peak at edge of valence band maximum (VBM). The Zndoped EDOSs in figure 3.2(c) showed that sizes of peaks as VBM and CBM (conduction band minimum) in ZB phase are reduced under the increasing pressure, and the energy gap is vanished in RS phase. For the doped of S, Si and Sn in figure 3.2(d), 3.2(e) and 3.2(f), we found that the increasing of high-pressure increases band gap from ambient condition. Sn-doped generates the implicit peak at VBM. Peaks of EDOS at VBM and CBM are flatted and extended along x-axis due to high-pressure effect. The primitive cell of the doped InP gets the stress from external forces under high-pressure condition. The external forces send effect on lattice constants and chemical bonds. Reducing of lattice constants sends effect on motion of electrons. As a result, available states are extended. The electrons EDOSs of all compounds in RS show non-semiconductor phase. Partial density of states (PDOSs) of the S, Si, Sn and Zn impurities in the InP host are compared in figure 3.3. The p-orbital is mainly available states in all doping. The Si and Sn-doped (IV-A group) gave similarly PDOS in the InP host, VBM shifted in the right-hand side (RHS) compared with Fermi level, while PDOS of S has shifted in the left-hand side (LHS). PDOS of Zn atom shows s, p and d orbitals of the transition element. The p-orbital-DOS of Sn at VBM and CBM of Sn reduced under high-pressure in ZB which related with EDOS. It has shifted in the RHS, and the gap was filled when changes to RS. To understand the chemical bonding and electron sharing between impurity and nearby atom, the electron density differences are compared in figure 3.4. Contour plot of electron density difference (EDD) shows the gradient of electron density due to two atoms are forming interactions from Blue zone = -0.15 to Red zone = +0.15. For the undoped InP as figure 3.4(a), (b), (c), (d), the EDD of In-P chemical bond is slowly increased in ZB.

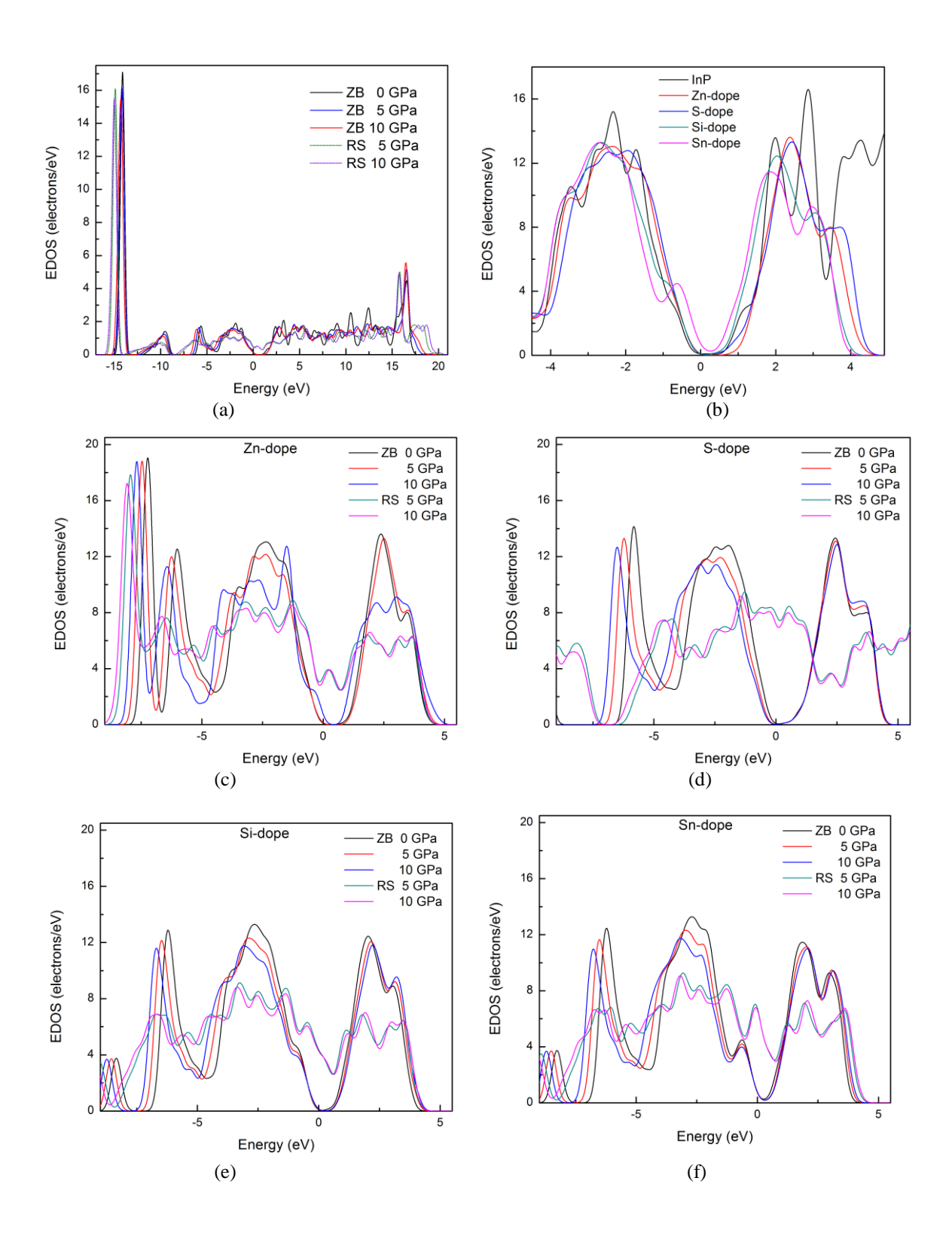


Figure 3.2: Electronic density of states of the doped InP under pressure. (a) InP at 0, 5 and 10 GPa in ZB and RS. (b) Comparison of doped and undoped InP at 0 GPa. (c) Zn-doped InP under pressure in ZB and RS. (d) S-doped InP under pressure in ZB and RS. (e) Si-doped InP under pressure in ZB and RS. (f) Sn-doped InP under pressure in ZB and RS.

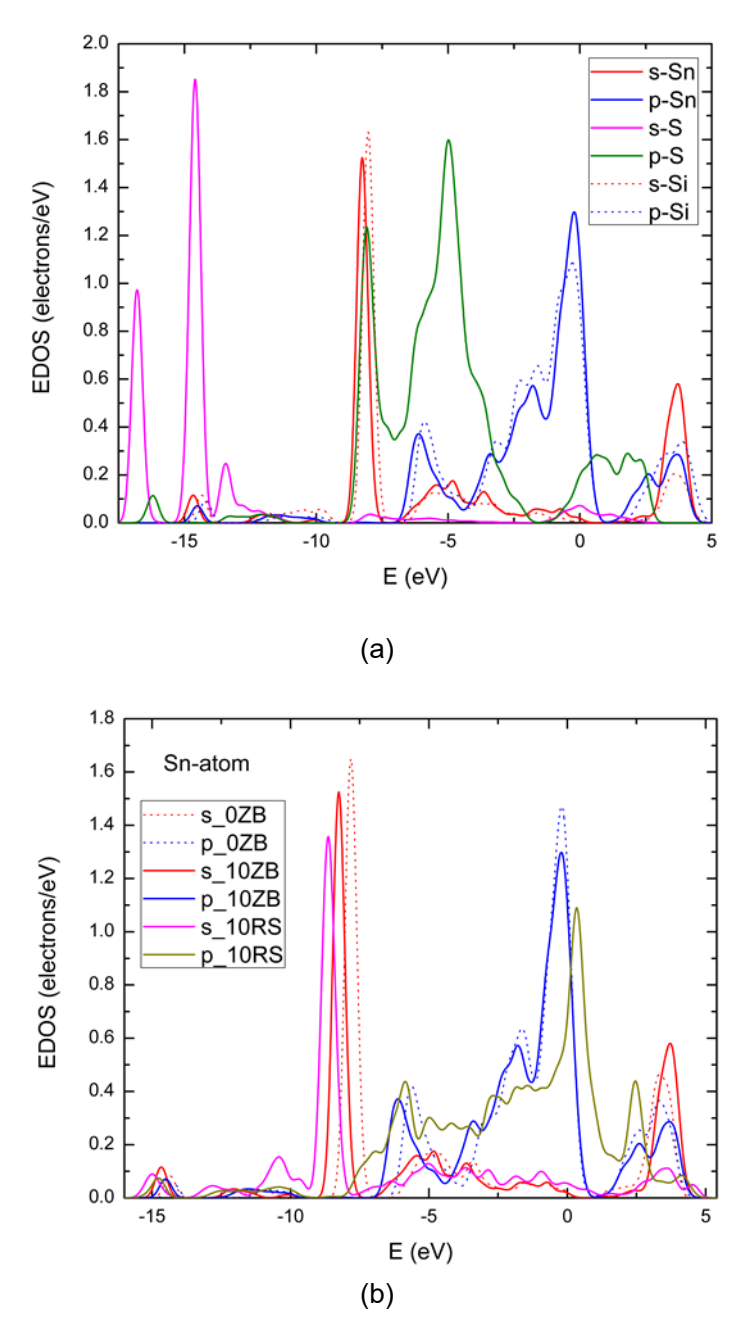


Figure 3.3: The partial density of states of impurity atoms (a) s and p orbitals of Sn, S and Si at 0 GPa. (b) s and p orbitals of Sn-atom in ZB (0,10 GPa) and RS (10 GPa).

Although the volume of unit cell is reduced by phase transition, the In-P bond length is 2.630 Å increased in RS that is larger than in ZB (2.435 Å), trying to reduce the stress and strain on cubic lattice. The sharing of electron density In-P in RS is reduced due to the bond length increasing as shown in table 3.4. In the doped compounds, the order of EDD is Zn-P>Si-In>S-In>Sn-In. Size of bond length as the same pressure is In-Sn>In-S>In-Si>In-P>Zn-P. The bond lengths in both ZB and RS phases are reduced under pressure increasing. The Zn-P bond in ZB has the strongest sharing electrons which related to the shortest bond length.

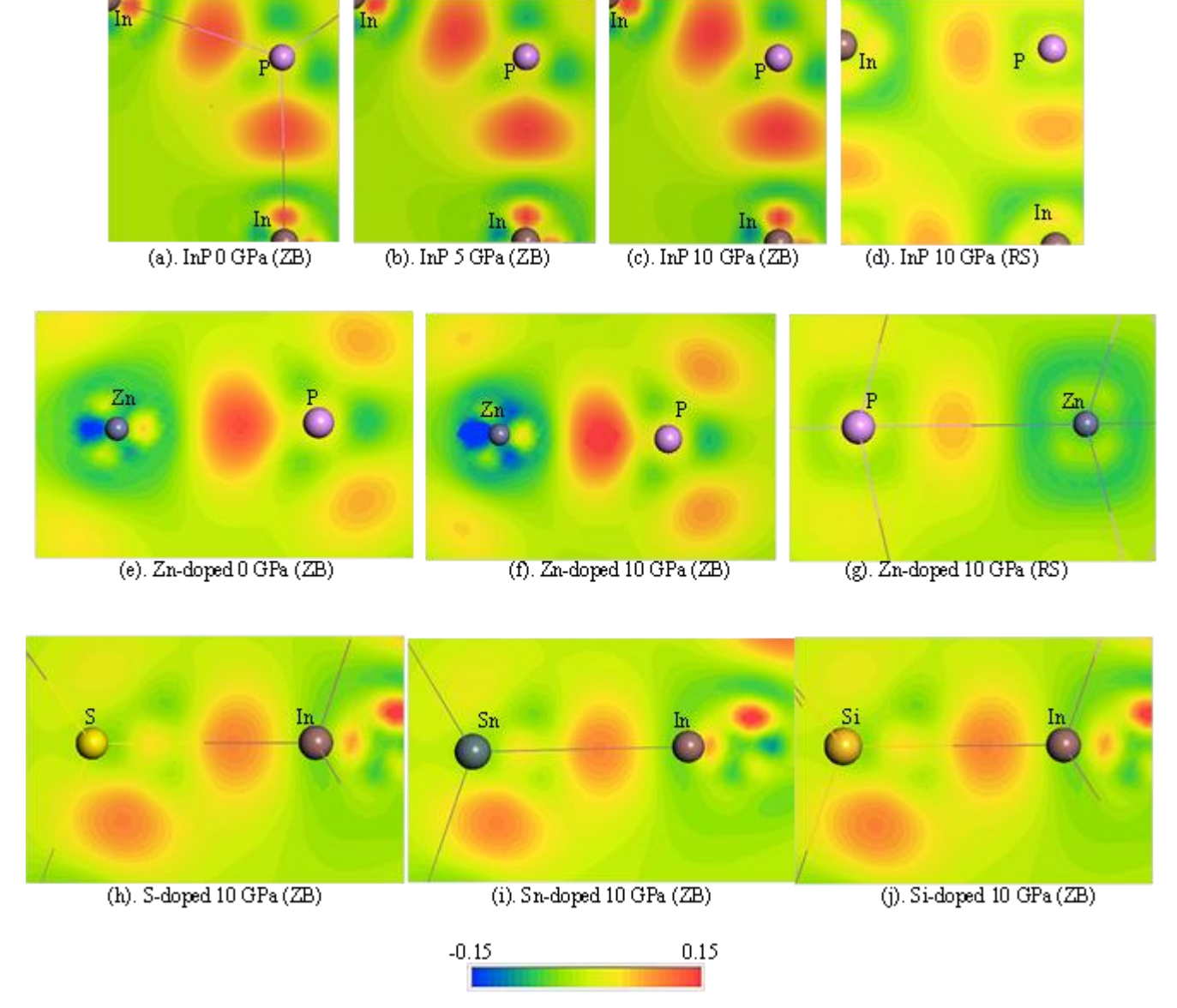


Figure 3.4: Electron density difference of doped and undoped InP under pressure.

Table 3.4: bond lengths of InP and impurities under pressure.

Structure	P (GPa)	Bond length (Å)					
		In-P	Zn-P	In-Si	In-Sn	In-S	
ZB	0	2.525	2.354	2.532	2.657	2.582	
	5	2.474	2.295	2.479	2.602	2.531	
	10	2.435	2.249	2.436	2.563	2.495	
RS	5	2.668	2.542	2.705	2.801	2.708	
	10	2.630	2.505	2.664	2.757	2.671	

#### 3.3 Optical properties

The optical properties and photo-absorption of the doped InP under pressure are investigated also. Probability of transition states from valence band to conduction band that translated the photo energy to the excited carrier concentration of semiconductor are compared by dielectric function. The real and imaginary parts of dielectric functions which are the basic parameters for generated all optical properties are presented, and compared with the experiment between the frequency range 0.5-6.0 eV [33] as shown in figure 3.5(a). The calculated dielectric functions have shifted in LHS, when compared with experiment (dot line), because of the lower estimated band gap from LDA result. However, the trends of two graphs are in consistent with experiment [33]. The calculated elastic functions of Zn-doped conditions in figure 3.5(b) are smooth functions more than InP. It has small shift on the positive frequency in RHS under 10 GPa. In range of low frequency 0-2 GPa, the imaginary part is dominated,  $\varepsilon_2 > \varepsilon_1$ . The dielectric performance is reduced by the doping effect due to the reducing of  $\varepsilon_2/\varepsilon_1$  ratio, and it transforms to conductor performance as high frequency.

Photoabsorption can be obtained from the dielectric function through the Kramers-Kronig relations [34]. Photo absorptions in wavelength between 200-850 nm in range of ultraviolet, visible light and infrared regions are presented in figure 3.6. In ZB phase, absorption coefficients are reduced by the doping and high-pressure effects. In RS phase, the absorption coefficients are highly increased but the compounds have become the non-semiconductor due to the closing of band gap. However, the calculated photo absorptions in the doped InP are focused only in the semiconductor phase (ZB) that the carrier transition through energy band gap. In figure 3.6(b), absorption coefficients of doped compounds are lower than undoped condition but there are increased at 250 nm. The values of photo-absorption coefficients in range of visible light of the impurities are Sn>Si>S>Zn. There are reduced by high pressure effect at 10 GPa. The tendency of photo-absorption is related to band gap and impurity peaks of EDOS. The peaks of VBM and CBM are flatted under high pressure, and the distance between the top of two peaks is increased under the pressure increasing as shown in figure 3.1(d), (e), (f); as a result, the probability transition from VBM to CBM and absorption coefficients are reduced.

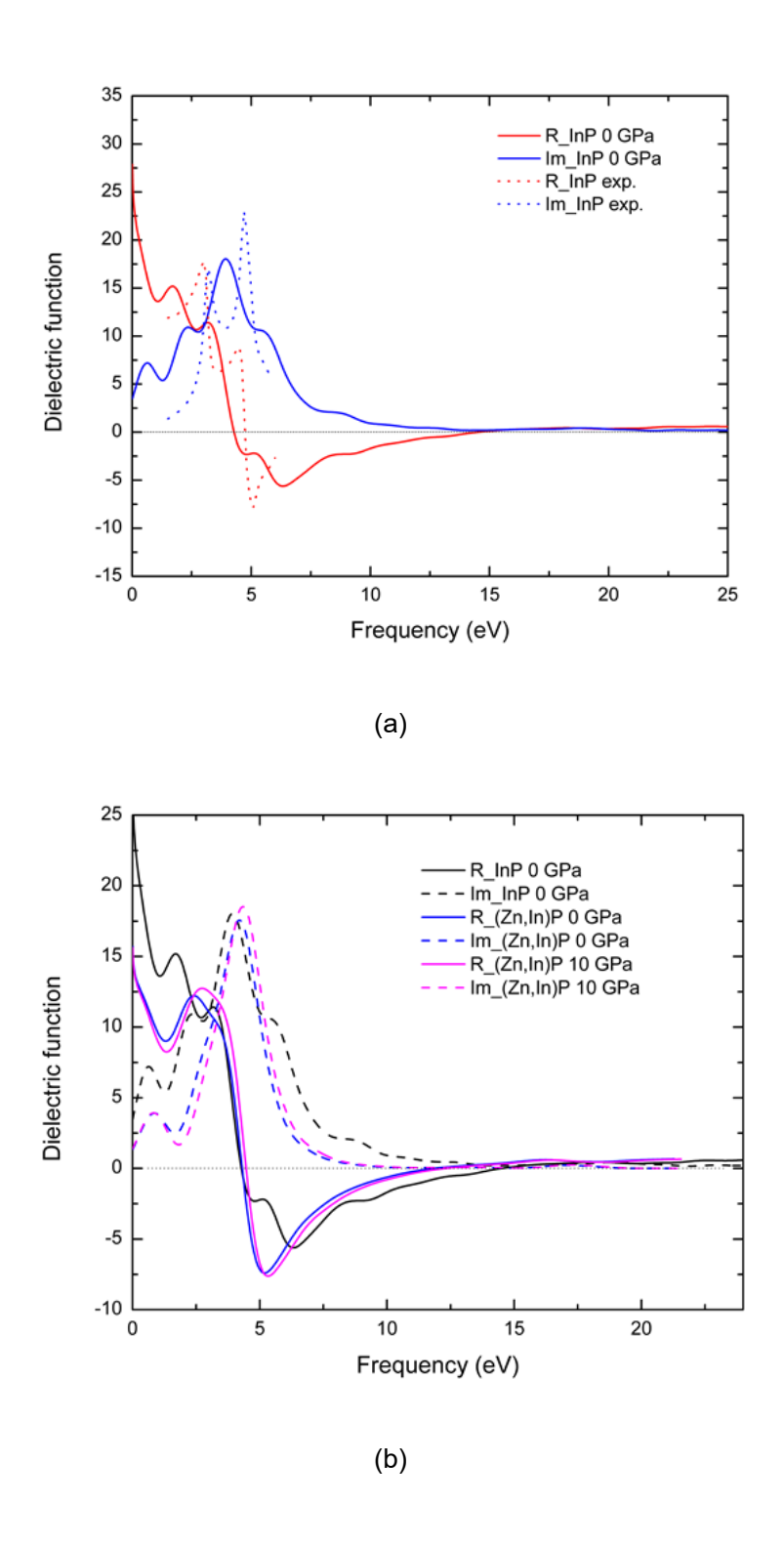


Figure 3.5: The calculated dielectric functions in real (R) and imaginary (Im) parts (a) comparing with the experiment result [33] (b) comparing with doping (In,Zn)P at 0 and 10 GPa.

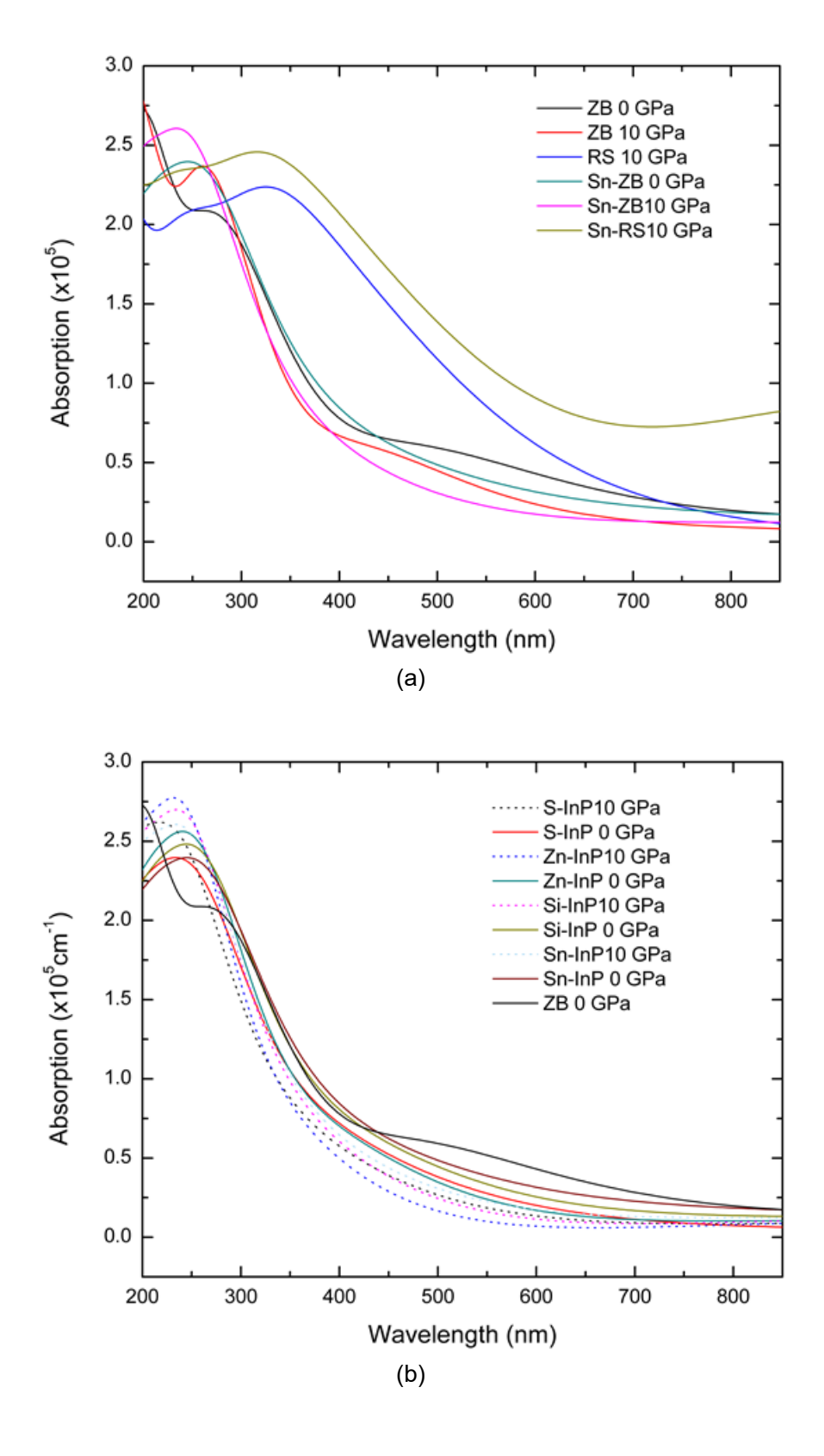


Figure 3.6: Photo absorptions of doped InP (a) comparison between undoped and Sndoped InP in ZB and RS. (b) Zn, S, Si, Sn-doped and undoped InP in ZB at 0 and 10 GPa.

#### 3.4 Mechanical properties

Elastic constants of the alloying conditions are calculated to investigate the mechanical properties of the doped InP under high-pressure. The elastic constants  $(c_{ij})$  can provide the hardness, stress and strain in each direction of external forces on a primitive cell of material. The calculated elastic constants of InP with the LDA-CAPZ, GGA-PBE and GGA-PBEsol functionals are compared with the previous experiment [6] as shown in table 5. The calculated results from LDA-CAPZ are in good agreement with the experiment [6], better than PBE and PBEsol. The elastic stiffness constants of InP satisfy the conditions of Born stability criteria in cubic structure (ZB and RS) [35, 36]:  $c_{11} + 2c_{12} > 0$ ,  $c_{44} > 0$ ,  $c_{11} - c_{12} > 0$ .

Table 3.5: Comparison the exchange-correlation functionals to calculate the elastic properties of InP at 0 GPa.

proportion of the detail							
Method	C <sub>11</sub>	C <sub>12</sub>	C <sub>44</sub>	В	G	Y	е
GGA-PBE	86.8	45.5	42.0	59.3	31.5	55.5	0.344
GGA-PBEsol	93.4	51.6	43.1	65.5	32.2	56.6	0.356
LDA-CAPZ	100.6	55.9	46.2	70.8	34.5	60.7	0.357
Exp. [6]	101	56	45	71	22.5	61	0.360

Bulk modulus (B), Shear modulus (S), Young's modulus (Y) and Poisson's ratio (v) can be obtained from  $c_{ij}$  based on VRH method [29, 30]. The upper and lower bounds of B and S in VRH scheme are  $B_{v}$ ,  $B_{R}$  and  $G_{v}$ ,  $G_{R}$ , respectively. For ZB and RS structures in cubic system [37],

$$\begin{split} B_V &= B_R = (1/3)(c_{11} + 2c_{12}), \\ G_V &= (1/5)(c_{11} - c_{12} + 3c_{44}), \\ G_R &= 5(c_{11} - c_{12})c_{44} / (3c_{11} - 3c_{12} + 4c_{44}). \end{split}$$

The bulk values (B, S, Y and v) are estimated by VRH approximation:

$$B = (B_V + B_R)/2,$$
  
 $G = (G_V + G_R)/2,$   
 $Y = 9BG/(3B+G),$   
 $V = (3B-2G)/(6B+2G).$ 

Table 3.6: Elastic parameters in a unit GPa (except  $\ensuremath{\varepsilon}$  ) of doping InP in ZB and RS.

Structure	condition	C <sub>11</sub>	C <sub>12</sub>	C <sub>44</sub>	В	G	Y	ε	B/G	$H_{V}$
ZB	InP	100.6	55.9	46.2	70.8	34.5	60.7	0.36	2.05	4.99
0 GPa	(In,Zn)P	87.6	63.0	30.6	71.2	21.2	57.1	0.42	3.36	2.02
	In(P,S)	86.7	51.6	32.8	63.3	25.5	46.3	0.37	2.48	3.24
	In(Si,P)	82.3	60.4	23.8	67.7	17.4	56.1	0.42	3.89	1.48
	In(Sn,P)	75.2	59.6	16.7	64.8	12.3	56.6	0.44	5.27	0.82
10 GPa	InP	139.1	100.5	44.4	113.4	31.8	54.9	0.42	3.56	2.51
	(In,Zn)P	125.2	108.1	23.8	113.8	15.6	103.3	0.46	7.29	0.67
	In(P,S)	124.3	99.3	28.7	107.6	20.6	93.9	0.44	5.22	1.20
	In(Si,P)	121.4	106.8	19.6	111.7	13.2	102.9	0.47	8.46	0.50
	In(Sn,P)	114.0	105.1	10.1	108.0	7.3	103.2	0.48	14.79	0.18
RS	InP	269.4	64.2	66.2	132.6	79.0	244.7	0.19	1.68	11.25
10 GPa	(In,Zn)P	264.2	76.1	24.1	138.8	43.2	110.0	0.22	3.21	3.51
	In(P,S)	251.2	74.1	30.0	133.1	47.1	101.7	0.23	2.83	4.32
	In(Si,P)	229.6	78.2	29.0	128.7	43.1	99.9	0.25	2.99	3.81
	In(Sn,P)	224.2	73.1	23.2	123.5	38.1	103.6	0.36	3.24	3.18

From the calculated B and G moduli, Chen et al. [41] proposed that Vickers hardness of polycrystalline materials can be estimated in terms of  $k = \frac{G}{R}$  and G in the form

$$H_V = 2(k^2G)^{0.585} - 3.$$

Nevertheless, Tian et al. [42] suggested that it may make the negative hardness for some low hardness materials due to the constant term "-3", so they modified new equation which can always give positive values for low hardness materials. Tian et al.'s correction which used in this work is

$$H_{V} = 0.92k^{1.137}G^{0.708}$$
.

The elastic parameters are shown in table 6 that the errors of  $c_{\scriptscriptstyle jj}$  calculations are less than 1 GPa. There are satisfied the Born stability criteria in all conditions [38, 39]. This indicates that structures of InP alloys are mechanically stable phases in ZB and RS. At ambient pressure, almost of B, Y and S of the InP alloys are smaller than of pure InP, especially the reducing of S. The critical B/G ratio of 1.75 separates type of ductile (>1.75) and brittle (<1.75) materials, which was introduced by Pugh [43]. While, Frantsevich et al. [44] suggested another critical ratio of B/G =2.67. Therefore, highvalue of the B/G ratio indicates ductility of material. When compare between pure and alloyed conditions at a given pressure, almost  $c_{11}$  are decreased by alloying elements, while  $c_{\rm 12}$  are increased. Therefore, the substitutions with Zn, S, Si and Sn can change the properties of InP to ductile material. The value of Y indicates ability of resistance from the external tensile-strength that Y of the alloyed conditions increases in ZB (10 GPa) but it reduces in RS at 10 GPa, when compared with ambient pressure. This supported that RS is high symmetry structure which gave high resistance from the perpendicular forces. The parameters of  $c_{11}$ ,  $c_{12}$  and B in ZB are increased under highpressure because of the reducing of bond length and primitive cell. High Poisson's ratio (>0.25) [45, 46] corresponds to the large deformation of volumetric change and high anisotropy as shown in ZB phase. While, Poisson's ratio of InP alloys in high-symmetry RS phase exhibit small deformation supported the higher isotropy, corresponding to high-symmetry cubic phase. High values of B, G and Y in RS in RS supported the packed atoms in high-symmetry system that it reduces the tangential stress. The B/G ratio in RS is lower than in ZB, indicating that ductility of InP alloys are reduced in RS. The estimated Vickers hardness from Tian et al.'s correction is listed in table 6. We can see that  $H_{\nu}$  of InP-ZB at ambient condition is 4.99 GPa, which is in good agreement with the experiment result (5.4 GPa) [41]. Tendency of  $H_{\nu}$  indicates that all impurities reduce hardness of pure InP.  $H_{\nu}$  decreases in ZB phase at high pressure (10 GPa) but it increases when transform to RS phase ( $H_{\nu}$  =11.25 GPa). The results of Vickers hardness in all compounds supported that RS phase is high symmetry structure because there are increased at the transition pressure of ZB-RS.

## **Chapter IV**

#### **Conclusions**

We study the structural and electronic properties of doped III-V binary compounds under extreme conditions. The high-pressure and temperature effects are interested in this work because these effects are the significant parameters for changing material properties. The III-V binary compounds are investigated because it was widely used in application devices. The charge carriers in intrinsic semiconductors can be changed by adding the doping effect on the host semiconductors.

Structural, electronic, optical and mechanical properties of Zn, Si, Sn and S substituted in InP supercell in ZB and RS structures are reported in Journal of Alloys and Compounds (2017) 700 98-105. Cohesive energy and enthalpy are observed, and indicated that In site is a preference site of Zn-alloyed, while a preference site of Sn, Si and S elements in InP is the P site. The possible spontaneous process in experimental growth which is introduced from  $H-H_0$  is (In,Zn)P > In(P,S) > In(Si,P) > In(Sn,P). The lower  $\Delta H$  in RS structure indicates that the spontaneous process of impurity substitution can be occurred in RS more than in ZB. For electronic structure, the porbital is mainly in available states in all compounds. Phase transition from ZB to RS reduces the strain on crystal lattice by the increasing of chemical bond length. Strength of In-P bond in ZB phase increases slowly under the increasing pressure (0, 5 and 10 GPa) which related with previous work [16], shown in figure 3.5. The bond length in ZB phase decreases under high-pressure, and electron density difference indicates the strong of bond at 10 GPa which supported N. Bouarissa's work. The chemical bonding of Zn-P in ZB is the strongest sharing electrons when compared with other compounds, Zn-P>Si-In>S-In>Sn-In. For optical properties, the dielectric performance compared from  $\varepsilon_2/\varepsilon_1$  ratio is reduced by the alloying effect, and it transforms to conductor performance at high frequencies. Effect of impurities on ability of photo-absorption in range of visible light is Sn>Si>S>Zn, and it reduces as the pressure increasing. Mechanical stability of InP alloys was observed, and satisfied the Born stability criteria. The impurities reduce Shear modulus of pure InP. Poisson's ratio of InP alloys in RS exhibit small deformation and high isotropy, corresponding to high-symmetry cubic phase. High values of B, G and Y in RS supported atomic structure in RS that packed in high-symmetry system. B/G ratio indicates that ductility of all alloys in RS is reduced,

when compared with ZB. The ductility of InP is induced by the alloying effect due to the *B/G* ratio increasing. High value of Vickers hardness in RS phase of all compounds supported that RS is high symmetry structure. High value of Vickers hardness in RS phase of all compounds supported that RS is high symmetry structure.

We expect that the fundamental data about the exact properties under extreme conditions of undoped and doped III-V compounds from this work can suggest the suitable conditions for application devices which are the advantages from this work. The novel information the extreme conditions obtained in this research. In future work, this technique will be applied on the properties of hydrogen storage materials.

In finally, we would like to thank the financial support from Thailand Research Fund (TRF) ID code TRG5880006, and Faculty of Science and Technology, Huachiew Chalermprakiet University. This work has been partially supported by National Research Council of Thailand. Computing facilities have been supported by Super SCI-II research grant, Faculty of Science and Ratchadaphiseksomphot Endowment Fund of Chulalongkorn University (CU-59-039-AM).

### References

- 1. G.J. Ackland, Rep. Prog. Phys. 64 (2001) 483.
- 2. I. Vurgaftman, J.R. Meyer, L.R. Ram-Mohan, J. Appl. Phys. 89 (2001) 5815.
- 3. N. Bouarissa, Physica B 406 (2011) 2583.
- 4. P.L. Souza, P.R. Ribas, J.V. Bellini, W.M. Mendes, J. Appl. Phys. 79 (1996) 3482.
- 5. C.S. Menoni, I.L. Spain, Phys. Rev. B 35 (1987) 7520.
- 6. D.N. Nichols, D.S. Rimai, R.J. Sladek, Sol. Stat. Comm. 36(8) (1980) 667.
- 7. A. Mujica, R.J. Needs, Phys. Rev. B 55 (1997) 9659.
- 8. H. Xue, F. Tang, W. Lu, Y. Feng, Z. Wang, Y. Wang, Comput. Mater. Sci. 67 (2013) 21.
- 9. P. Pluengphon, T. Bovornratanaraks, Sol. Stat. Comm. 218 (2015) 1.
- 10. M. Durandurdu, D.A.Drabold, Phys.Rev.B:Condens.Matter 66 (2002) 045209.
- P. Pluengphon, T. Bovornratanaraks, S. Vannarat, U. Pinsook, Solid State Commun.
   195 (2014) 26.
- 12. Y. Zhao, H. Hou, Y. Zhao, P. Han, J. Alloys Compd. 640 (2015) 233.
- 13. J. Long, C. Shu, L. Yang, M. Yang, J. Alloys Compd. 644 (2015) 638.
- 14. Y. Xu, C. Chen, S. Wang, X. Sun, J. Alloys Compd. 669 (2016) 101.
- 15. N. Bouarissa, Solid-State Electronics 44 (2000) 2193.
- 16. N. Bouarissa, Materials Chemistry and Physics 65 (2000) 107.
- 17. N. Bouarissa, Infrared Physics & Technology 40 (1999) 117.
- 18. Y. Moon, S. Si, E. Yoon, S.J. Kim, J. Appl. Phys. 83 (1998) 2261.
- 19. E.F. Schubert, C.J. Pinzone, M. Geva, Appl. Phys. Lett. 67(5) (1995) 700.
- J. Decobert, D. Herrati, V. Colson, D. Leclerc, L. Goldstein, J. Crystal Growth 248
   (2003) 390.
- 21. S.B. Youssef, Physica A 235 (1997) 334.
- 22. H. Hu, X. Wu, R. Wang, Z. Jia, W. Li, Q. Liu, J. Alloys Compd. 666 (2016) 185.
- 23. Y. Hu, S. Shang, Y. Wang, et al., J. Alloys Compd. 671 (2016) 267.
- M.C. Payne, M.P. Teter, D.C. Allan, T.A. Arias, D. Joannopoulos, Rev. Mod. Phys.
   (1992)1045.

- 25. M.D. Segall, P.L.D. Lindan, M.J. Probert, C.J. Pickard, P.J. Hasnip, S.J. Clark, M.C. Payne, J. Phys.: Condens. Matter 14 (2002) 2717.
- 26. J.P. Perdew, J.A. Chevary, S.H.Vosko, K.A. Jackson, M.R.Pederson, D.J. Singh, C. Fiolhais, Phys. Rev. B 46 (1992) 6671.
- 27. J.P. Perdew, K. Burke, M. Ernzerhof, Phys. Rev. Lett. 77 (1996) 3865.
- 28. D. Vanderbilt, Phys. Rev. B 41 (1990) 7892.
- 29. H.J. Monkhorst, J.D. Pack, Phys. Rev. B 13 (1976) 5188.
- 30. B.G. Pfommer, M. Cote, S.G. Louie, M.L. Cohen, J. Comput. Phys. 131 (1997) 233.
- 31. R.P. Feynman, Phys. Rev 56 (4) (1939) 340.
- 32. R. Hill, Proc. Phys. Soc. A 65 (1952) 349.
- 33. G.V. Sinko, N.A. Smirnov, J. Phys.: Condens. Matter 14 (2002) 6989.
- 34. L. Li, Q. Gao, G. Lei, H. Xie, J. Deng, Xian-Ru Hu, J. Phys. Chem. Solids 94 (2016) 30–36.
- 35. P. Pluengphon, T. Bovornratanaraks, S. Vannarat, U. Pinsook, J. Phys.: Condens. Matter 24 (2012) 095802.
- 36. D.E. Aspnes, A.A. Studna, Phys. Rev. B 27 (1983) 985.
- 37. R.F. Egerton (1996). Electron energy-loss spectroscopy in the electron microscope (2nd ed.). New York: Plenum Press. ISBN 0-306-45223-5.
- 38. B.B. Karki, G.J. Ackland, J. Crain, J. Phys.: Condens. Matter 9 (1997) 8579.
- 39. F. Mouhat, F.X. Coudert, Phys. Rev. B 90 (2014) 224104.
- 40. X. Zhang, W. Jiang, J. Alloys Compd. 663 (2016) 565.
- 41. X.Q. Chen, H. Niu, D. Li, Y. Li, Intermetallics 19 (2011) 1275.
- 42. Y.J. Tian, B. Xu, Z.S. Zhao, Int. J. Refract. Met. Hard Mater. 33 (2012) 93.
- 43. S.F. Pugh, Philos.Mag. 45 (1953) 833.
- 44. I.N. Frantsevich, F.F.Voronov, S.A.Bokuta, Elastic Constants and Elastic Moduli for Metals and Insulators Handbook, Naukova Dumka, Kiev (1983).
- 45. S. Aydin, M. Simsek, J. Alloys Compd. 509 (2011) 5219.
- 46. C. Li, K. Zhang, J. Ru, J. Alloys Compd. 647 (2015) 573.

### **Appendix**

**International Publication** 

### Output จากโครงการวิจัยที่ได้รับทุนจาก สกว.

- 1. ผลงานตีพิมพ์ในวารสารวิชาการนานาชาติ (ระบุชื่อผู้แต่ง ชื่อเรื่อง ชื่อวารสาร ปี เล่มที่ เลขที่ และหน้า) หรือผลงานตามที่คาดไว้ในสัญญาโครงการ

  <u>Prayoonsak Pluengphon</u>, Thiti Bovornratanaraks, Udomsilp Pinsook,

  Journal of Alloys and Compounds, (2017) vol.700 page 98-105.
- 2. การนำผลงานวิจัยไปใช้ประโยชน์
  - เชิงพาณิชย์ (มีการนำไปผลิต/ขาย/ก่อให้เกิดรายได้ หรือมีการนำไปประยุกต์ใช้ โดยภาคธุรกิจ/บุคคลทั่วไป)
  - เชิงนโยบาย (มีการกำหนดนโยบายอิงงานวิจัย/เกิดมาตรการใหม่/เปลี่ยนแปลง ระเบียบข้อบังคับหรือวิธีทำงาน)
  - เชิงสาธารณะ (มีเครือข่ายความร่วมมือ/สร้างกระแสความสนใจในวงกว้าง) ---
  - เชิงวิชาการ (มีการพัฒนาการเรียนการสอน/สร้างนักวิจัยใหม่)
     สามารถนำงานวิจัยพื้นฐานไปใช้ในการประกอบการเรียนการสอนรายวิชา
     Many-body problem, Density functional theory and Solid state physics
- 3. อื่นๆ (เช่น ผลงานตีพิมพ์ในวารสารวิชาการในประเทศ การเสนอผลงานในที่ประชุม วิชาการ หนังสือ การจดสิทธิบัตร)
  - 3.1 Poster Presentation in ASTC2016 26 May 2016 in the topics "High Pressure Phases of InP Calculated Using Density Functional Theory"
    3.2 Poster Presentation in Siam Physics Congress (SPC2016) 8-10 June 2016 in the topics "Phase Stability and Mechanical Properties of In(P,S) under Pressure: First-Principles Calculation"

ELSEVIER

Contents lists available at ScienceDirect

### Journal of Alloys and Compounds

journal homepage: http://www.elsevier.com/locate/jalcom



### Structural, electronic, optical and mechanical properties of InP alloyed with Zn, Si, Sn and S under pressure: First-principles calculation



Prayoonsak Pluengphon a, c, \*, Thiti Bovornratanaraks b, c, \*\*, Udomsilp Pinsook b, c

- <sup>a</sup> Division of Physical Science, Faculty of Science and Technology, Huachiew Chalermprakiet University, Samutprakarn, 10540, Thailand
- b Extreme Conditions Physics Research Laboratory, Department of Physics, Faculty of Science, Chulalongkorn University, Bangkok, 10330, Thailand
- <sup>c</sup> ThEP Center, CHE, 328 Si-Ayuttaya Road, Bangkok, 10400, Thailand

### ARTICLE INFO

Article history:
Received 23 November 2016
Received in revised form
28 December 2016
Accepted 6 January 2017
Available online 7 January 2017

Keywords: Phase stability Elastic properties InP alloys High pressure Ab initio method

### ABSTRACT

Structural, electronic, optical and mechanical properties of Zn, Si, Sn and S substitutions on InP supercell under pressure in zinc blende (ZB) and rock salt (RS) phases are presented using first-principles method. Cohesive energy and enthalpy difference are observed, and found that the order of possible spontaneous process in experimental growth, which introduced from enthalpy difference, is (In,Zn) P > In(P,S) > In(Si,P) > In(Sn,P). The lower enthalpy difference in RS structure indicates that the spontaneous process of impurity substitution can be occurred in RS more than in ZB. Phase transition from ZB to RS reduces the strain on crystal lattice by the increasing of chemical bond length. The chemical bonding of Zn-P in ZB is the strongest sharing electrons when compared with other compounds, Zn-P>Si-In>S-In>Sn-In. The dielectric performance of InP is reduced by the alloying effect, and it transforms to the conductor performance as high frequencies. Order of photo-absorption coefficient in range of visible light with the impurities is Sn>Si>S>Zn, and it reduces under high-pressure. Mechanical stability of InP alloys was observed, and satisfied the Born stability criteria. The impurities reduce Shear modulus of pure InP. Poisson's ratio of InP alloys in RS exhibit small deformation and high isotropy, corresponding to high-symmetry cubic phase. B/G ratio indicates that ductility of InP alloys is reduced, when it transformed to RS. The ductility of InP is induced by the alloying effect due to the B/G ratio increasing.

© 2017 Elsevier B.V. All rights reserved.

### 1. Introduction

During the last decades, the alloys and compounds of III-V binary semiconductors are great of interest for many applications on the electronic devices such as light emitting diodes, optoelectronic devices and photovoltaic materials. The efficiency of solar cell highly depends on the electronic and optical properties of the semiconductor materials in multilayer films. Indium Phosphide (InP) is one of most promising materials in a III-V group which used as a substrate for epitaxial growth applied in photovoltaic multilayers [1–3]. InP is widely used in high-frequency and high-power electronic devices because it has superior electron velocities and

 $\hbox{\it E-mail addresses: } prayoonsak@gmail.com (P. Pluengphon), thiti.b@chula.ac.th (T. Bovornratanaraks).$ 

long-lived optical phonons when compared with other III-V compounds [3,4]. Stable crystal structure of InP at ambient pressure (0 GPa) is zinc blende (ZB) in space group F-43m [5–7], which related with most of III-V semiconductors such as GaAs, GaN, InAs and InSb. When high-pressure in order of gigapascal (GPa) presses on a primitive cell, the stable structure of InP has the transformations each pressure range as  $F-43m \rightarrow Fm$ in  $3m \rightarrow Cmcm \rightarrow Immm \rightarrow Pm-3m$  at 5.6, 11.0, 50.0 and 102.0 GPa, respectively [7]. The 2nd phase of InP is rock salt (RS) phase in space group Fm-3m. The 1st transformation path from ambient phase to RS normally deforms to non-semiconductor due to the reconstruction bonding of disorder to order structures during phase transition that found in CuGaSe<sub>2</sub> [8,9] and GaAs [10,11]. Highpressure condition and structural phase transition have highly effected on chemical bond, band structure, electronic density of state (EDOS), photo absorption, elasticity and superconductivity [12–14]. Bouarissa studied high-pressure effects on the properties of InP, including electronic and optical properties [15], valence and conduction charge densities [16], and bonding and iconicity [17]. It was found that electronic charge densities are sensitive to the effect

<sup>\*</sup> Corresponding author. Division of Physical Science, Faculty of Science and Technology, Huachiew Chalermprakiet University, Samutprakarn, 10540, Thailand. \*\* Corresponding author. Extreme Conditions Physics Research Laboratory, Department of Physics, Faculty of Science, Chulalongkorn University, Bangkok, 10330, Thailand.

of hydrostatic pressure and the transverse effective charge decreases with increasing pressure which indicates the increased covalent bonding in the InP. In addition, the effects of impurity atoms on InP at ambient pressure have widely studied because the electronic and optical properties respond significantly with the concentration of impurities [18-23]. Zn-doped InP layers were obtained by in situ doping in low pressure metalorganic chemical vapor deposition, and thermal diffusion from a Zn-containing film [18]. Band edge peaks and band of shallow donor to acceptor transition peak were observed in in situ Zn-doped InP, implying that interstitial Zn atoms were generated during in situ doping. Schubert et al. [19] reported that Zn diffusion depends strongly on the concentration of Zn. Zn-doped is preferable in InP over other p-type dopants because it has high electrical activity, moderate diffusion, controllable incorporation and low residual toxicity. And then, the incorporation and doping process of Si, S and Zn impurities in InP by metalorganic vapor phase epitaxy have been studied both standard growth conditions and selective area growth conditions [20]. It was found that Zn-S co-doping shows a Zn dopant concentration enhancement in selective area growth conditions, while it remains constant in standard growth conditions. The Si concentration was unexpectedly independent of the growth rate in selective area growth conditions. Youssef [21] studied optical properties of Zn-doped InP, and found that Zn-doped increases refractive index and reduces band gap of InP.

From the literature review, we can see that the physical properties of both doped and undoped InP are widely studied at ambient pressure. However, high-pressure properties, including formation energies, free energy differences, electronic structures, optical properties and mechanical properties, on the InP with impurities are still incomplete. High-pressure technique is a vivid choice to change physical properties of condensed matters because it has high effect on atomic structures in scale of primitive cell. The electronic, optical and mechanical properties depend on the changed atomic structures under high-pressure. InP and their compounds are widely used in multilayer solar cell applications which ability of photovoltaic process based on these properties. Therefore, the high-pressure properties of Zn, Si, Sn and S substituted on InP calculated from first-principles calculation are presented and discussed in this report.

### 2. Calculation details

The first-principles calculations based on density functional theory (DFT) are performed to solve the Kohn-Sham equations by self-consistent field method (SCF) [24] as implemented in Cambridge Serial Total Energy Package (CASTEP) code [25]. To study DFT calculations in the alloyed InP systems, the local density approximation schemes of Ceperley-Alder-Perdew-Zunger (LDA-CAPZ) and the generalized-gradient approximation functional of Perdew-Burke-Ernzerhof (GGA-PBE) [26,27] are compared at ambient condition for finding the suitable exchange-correlation functional term in Kohn-Sham equations. In Table 1, we can see that lattice parameters and bulk modulus of InP calculated from LDA-CAPZ functional are better than GGA-PBE results; therefore, LDA-CAPZ

**Table 1** Lattice parameters (a = b = c), volume cell (V) and bulk modulus ( $B_0$ ) at 0 GPa in ZB structure of InP compared with previous studies [3,6].

a (Å)	$V(Å^3)$	B <sub>0</sub> (GPa)	Method	Ref.
5.968	212.6	59.3	GGA-PBE	This work
5.832	198.4	71.8	LDA-CAPZ	This work
5.869	202.2	71.0	EPM	[3]
5.856	200.8	71.1	Experiment	[6]

is mainly used as exchange-correlation functional for finding the high-pressure properties of the alloyed InP systems. This supported the DFT results in ZB structure (in Fig. 1) of GaAs (III-V) semiconductor in previous work [11].

To study the InP alloys, the impurity atoms which consist of Zn. Si. Sn and S are substituted on In (or P) site in 1/8 of InP with super cell size  $2 \times 2 \times 2$  as shown in Fig. 1(c) and (d). The maximum energy of plane wave basis set used at 450 eV, which is suitable cutoff energy to cooperate with ultrasoft-pseudopotential [28]. Monkhorst-Pack grid sizes [29] for  $2 \times 2 \times 2$  super cells both ZB and RS structures are  $8 \times 8 \times 8$ , while k point in undoped InP initially finites as the condition of  $1/k \approx 0.035$ . The Brodyden-Fletcher-Goldfarb-Shanno (BFGS) [30] minimization scheme is used in geometry optimization. External forces and pressure tensors on optimized structures are controlled by Hellmann-Feynman theorem [31]. The BFGS optimization was considered to be completed when the total energy difference was less than  $2 \times 10^{-6}$  eV/atom, Hellman-Feynman forces were less than 0.006 eV/Å, the maximum ionic displacement within 0.0002 Å, and all of the stress components within 0.003 GPa. The average isotropic moduli in bulk obtained from elastic constants by Voigt-Reuss-Hill (VRH) method [32,33].

### 3. Results and discussion

### 3.1. Site preference and phase stability

In order to understand the structural features of the InP alloys, it is investigated by considerations the cohesive energy ( $E_{coh}$ ), which is a measure of the strength of atomic forces in solid state. The cohesive energy can be obtained from the difference between the average energy of the free atoms and that of a solid, which is correlated with the structural stability in ground state. The cohesive energy per formula unit (eV/f.u.) of the compounds  $In_{1-x}M_xP$  or (In,M)P can be calculated in form [34]

$$E_{coh} = (1-x)E_{atom}^{ln} + xE_{atom}^{M} + E_{atom}^{P} - E_{total}^{(In,M)P} \label{eq:ecoh}$$

While cohesive energy per formula unit of the compound  $InM_{x}P_{1-x}$  or In(M,P) is

$$E_{coh} = E_{atom}^{ln} + x E_{atom}^{M} + (1 - x) E_{atom}^{P} - E_{total}^{ln(M,P)}$$

where  $E_{total}^{(In,M)P}$  and  $E_{total}^{In(M,P)}$  are the total energies per formula unit of the (In,M)P and In(M,P) compounds,  $E_{atom}^{In}$ ,  $E_{atom}^{M}$  and  $E_{atom}^{P}$  are the energies of In, M and P of isolated constituent atoms (M = Zn, S, Si and Sn). The cohesive energies at ambient pressure are analyzed as shown in Table 2. We also compare Gibbs's free energy of system (G = E + PV - TS) which G = E + PV = H at T = 0 K. The free energy differences  $(H - H_0)$  can be obtained from free energies of the alloyed InP compounds (H) based on that of pure InP  $(H_0)$ .

The results supported well-kwon knowledge that site preference of Zn (II-B) impurity is the In site, while S (VI-A) atom prefers to substitute on P site, depending on position of elements and electronegativity values in periodic table. The positive cohesive energies of (In,Zn)P and In(P,S), which are 8.32 and 8.34 eV/f.u., show the structural stability in solid form of the InP alloys. When we compare free energies of alloys based on pure InP, the negative free energies  $(H-H_0<0)$  supported stability of (In,Zn)P and In(P,S)compounds. It is indicated that the Si and Sn impurities (IV-A group) prefer to substitute on the super cell of InP in the forms of In(Si,P) and In(Sn,P). Therefore, site preferences of alloying InP with Zn, S, Si and Sn are (In,Zn)P, In(P,S), In(Si,P) and In(Sn,P), respectively. The possible spontaneous process in experimental growth can be suggested from  $H-H_0$ which (In.Zn)

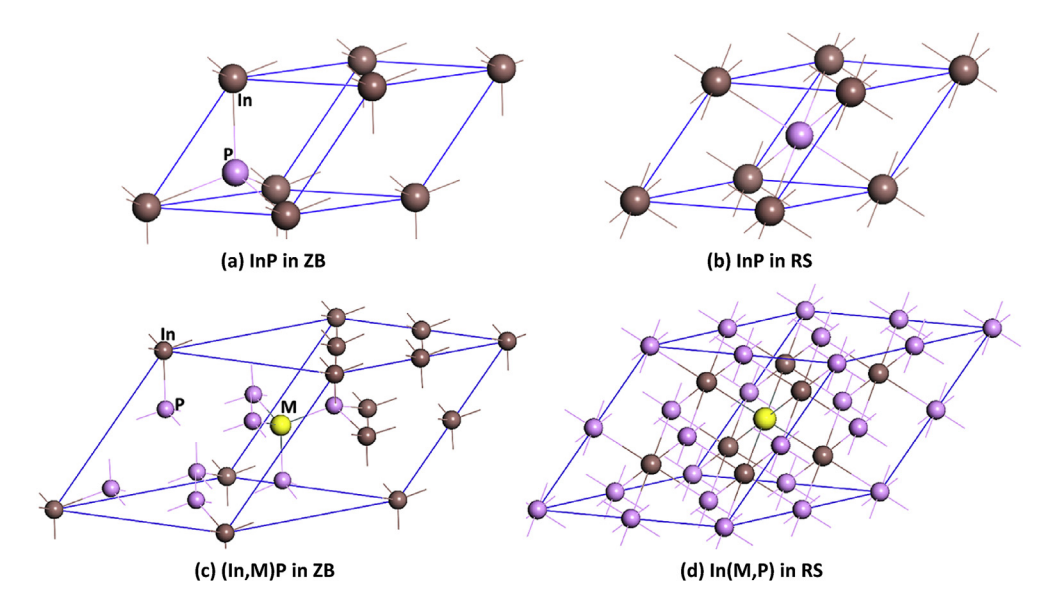


Fig. 1. Atomic structures of InP in pure and alloys conditions (a) InP in ZB structure (b) InP in RS structure (c) InP replaced by M atom in ZB supercell (d) InP replaced by M atom in RS supercell.

**Table 2**Comparisons cohesive energy and free energy difference of InP alloys at 0 GPa.

Compound	InP	(In,Zn)P	In(P,S)	(In,Si)P	In(Si,P)	(In,Sn)P	In(Sn,P)
$E_{coh}$ (eV/f.u.)		8.32	8.34	8.72	8.32	8.54	8.14
$H-H_0$ (eV/f.u.)		-18.52	-12.24	181.86	9.28	183.34	10.76

P > In(P,S) > In(Si,P) > In(Sn,P) as shown in Table 2.

To compare the possible spontaneous process in ZB and RS phases, free energies of the (In,Zn)P, In(Si,P), In(Sn,P) and In(P,S) compounds under pressure are observed and compared with InP as shown in Table 3. The calculated phase transition from ZB to RS occurred at 10–12 GPa that are in consistent with previous works [1,7]. The effect of impurity has small effect on the transition pressure [35]. We found that the increasing of pressure in ZB from 5 to 10 GPa has small effect on  $\Delta H = H - H_{InP}$ , while it reduces significantly during phase transformation from ZB to RS in all alloys. The lower  $\Delta H$  in RS indicates that the spontaneous process of impurity substitution can be occurred in RS more than in ZB.

### 3.2. Electronic properties

The EDOSs of (In,Zn)P, In(Si,P), In(Sn,P) and In(P,S) are analyzed to understand the effects of high-pressure and phase transition on the InP alloys in ZB and RS. In Fig. 2(a), we found that band gap of InP appears only in ZB phase (0, 5 and 10 GPa), where Fermi level is set at zero energy and denoted by the vertical dash-line. But the gap is vanished in RS structure both 5 and 10 GPa. The closed band gap

**Table 3**Free energy differences of the (In,Zn)P, In(P,S), In(Si,P) and In(Sn,P) alloys based on InP in ZB and RS phases under pressure 0, 5 and 10 GPa.

Structure	P (GPa)	$H_{InP}$ (eV/f.u.)	$H-H_{InP}$ (eV/f.u.)				
		InP	(In,Zn)P	In(Si,P)	In(Sn,P)	In(P,S)	
ZB	0	-1740.80	-18.52	9.28	10.76	-12.24	
	5	-1739.20	-18.58	9.28	10.82	-12.20	
	10	-1737.68	-18.62	9.30	10.86	-12.18	
RS	5	-1738.84	-18.74	6.18	7.48	-12.56	
	10	-1737.60	-18.78	6.10	7.44	-12.56	

occurred due to the difference of chemical bonds and number of neighbor atoms in ZB and RS. It is well known that high-pressure effect can change structure of InP from ZB to RS, and semiconductor properties (in ZB) will be changed to non-semiconductor (in RS) [1,7]. The peaks near valence band maximum (VBM) and conduction band minimum (CBM) are observed in Fig. 2(b). It is seen that the alloying with Si and Sn reduce band gap of InP, and generate the impurity peak at VBM. The EDOSs of (In,Zn)P in Fig. 2(c) indicate that the peaks at VBM and CBM in ZB phase are reduced when pressure increases, and the energy gap still disappears in RS phase. For comparisons of alloying with S, Si and Sn as shown in Fig. 2(d), (e) and 2(f), we found that the peaks of EDOSs at VBM and CBM under the increasing of pressure are reduced and spread out in x-axis. EDOSs of In(Sn,P) and In(Si,P) appear new peak at VBM, while it is not found in In(P,S). Available states of EDOSs at 5 and 10 GPa are extended along energy-axis because the carriers receive the stimulated energies from the external forces or highpressure. Partial density of states (PDOSs) of InP alloys are presented in Fig. 3, and found that *p*-orbital is mainly as available states in all alloys. The Si and Sn, which are impurities in IV-A group, gave similar distribution of PDOS. VBM of In(Si,P) and In(Sn,P) had shifted on the right-hand side compared with Fermi level, while PDOS of S has shifted in the opposite way. PDOS of Zn atom shows s, p and d orbitals of the transition element. The p-orbital of Sn at VBM and CBM reduced under high-pressure in ZB which related with EDOS. It has shifted in right-hand side, and the gap is closed in RS. The population analysis indicates that Zn atom in InP gave the p-d hybridization, while Si, S and Sn atoms gave the hybridization of s-p. To understand the chemical bonding and electron sharing between impurity and nearby atoms, the electron density differences are investigated in Fig. 4. The electron density difference that indicates electron delocalization in solid can be obtained from the difference between the self-consistent valence charge density and the superposition of atomic valence densities. It is useful for illustrating how chemical bonds are formed across the whole system as the electron density difference can help identifying the types of chemical bonds. Contour plot divides the gradient of electron density difference between Blue zone = -0.15 and Red zone = +0.15. Strength of In-P bond in ZB phase increases slowly under the increasing pressure (0, 5 and 10 GPa) which related with previous work [16], shown in Fig. 4(a), (b) and (c). But it is seen that

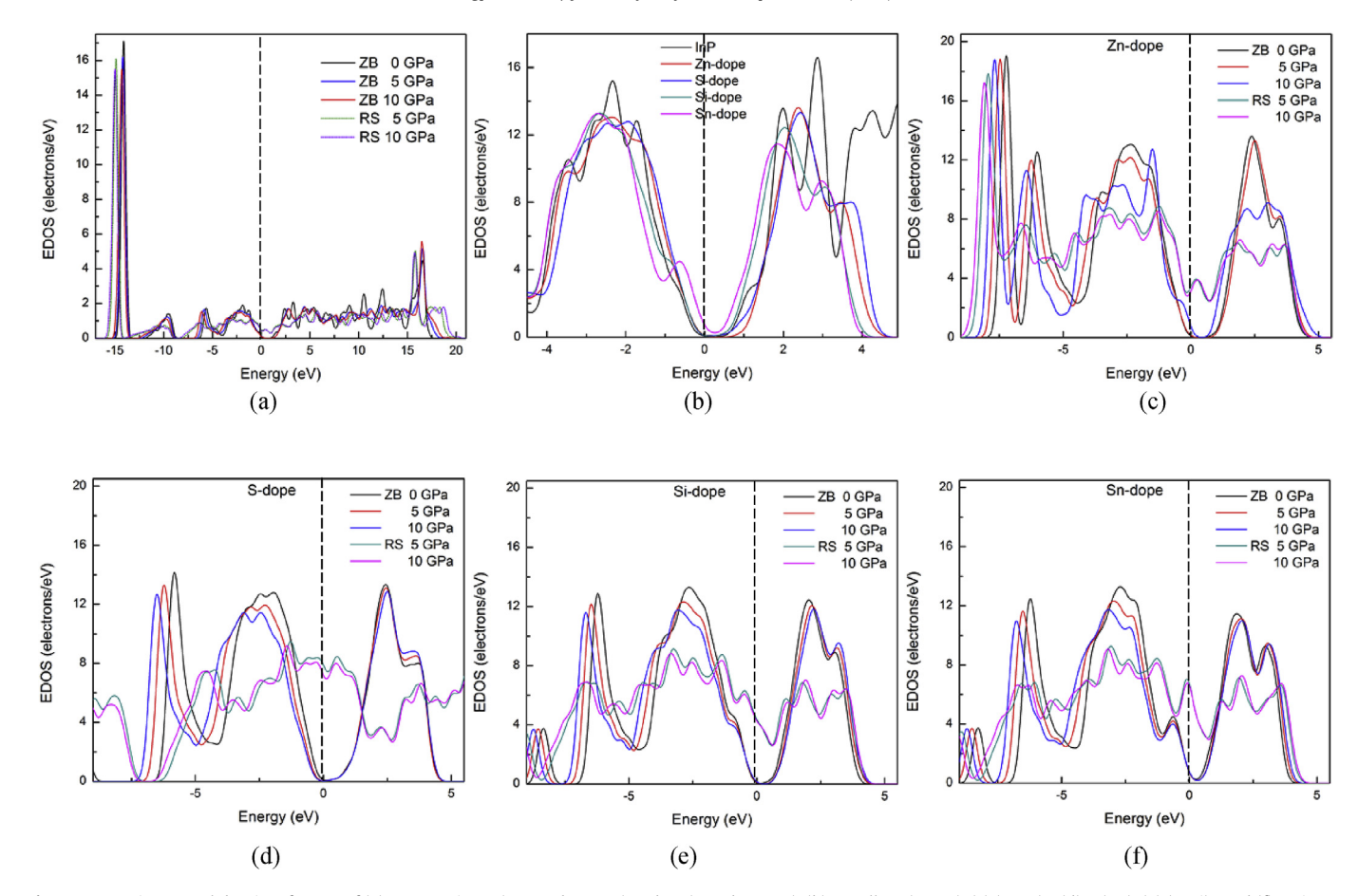
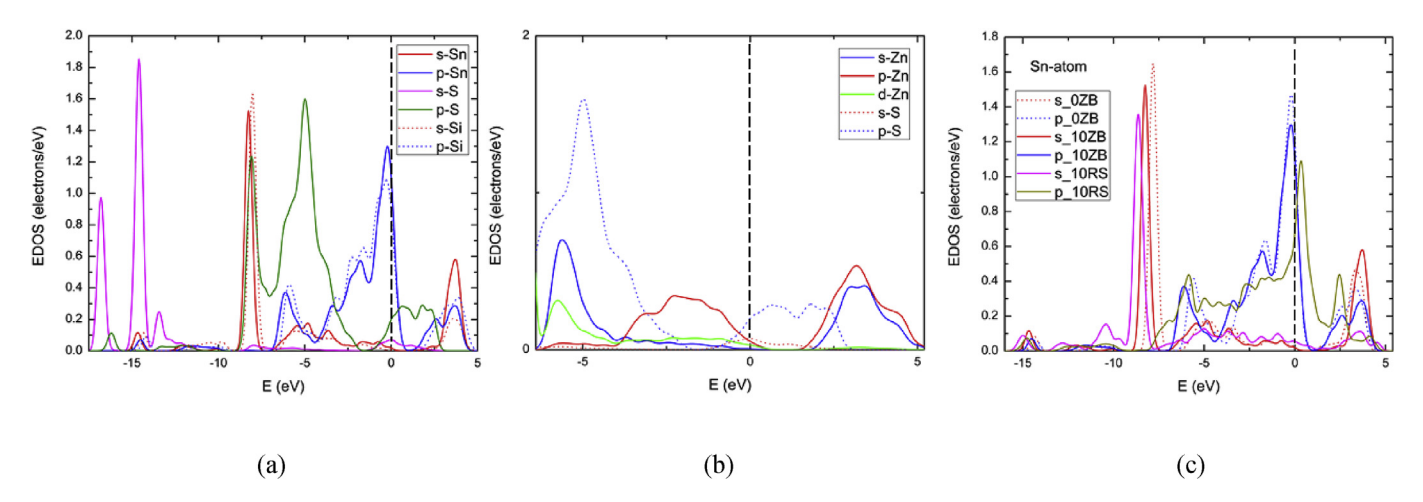


Fig. 2. Comparisons total density of states of (a) pure InP in ZB (0, 5 and 10 GPa) and RS (5 and 10 GPa), (b) InP alloys (0 GPa), (c) (In,Zn)P, (d) In(P,S), (e) (In,Si)P and (f) Sn in InP under pressure in ZB and RS.



**Fig. 3.** Partial density of states of impurity atoms (a) s and p orbitals of Sn, S and Si at 0 GPa. (b) s, p, d orbitals of Zn and S at 0 GPa. (c) s and p orbitals of Sn-atom in ZB (0 and 10 GPa) and RS (10 GPa).

structural phases of InP is relaxed when transforms to RS phase in Fig. 4(d). Although the volume cell is reduced by phase transition from ZB to RS, the covalent bond of In-P is weakened in RS phase due to the increasing of bond length 2.630 Å that larger than in ZB (2.435 Å). The increasing of bond length under volume reducing in InP system is occurred because it is trying to reduce the stress and strain on lattice by phase transition. The sharing of electron density In-P in RS is related to the bond length increasing as shown in

Table 4. For InP alloyed with elements, order of strong covalent bonding is Zn-P>Si-In>S-In>Sn-In, while bond length as the same pressure is In-Sn>In-S>In-Si>In-P>Zn-P. The bond length in ZB phase decreases under high-pressure, and electron density difference indicates the strong of bond at 10 GPa which supported N. Bouarissa's work [17]. The contour plots showed that Zn-P bond in (In,Zn)P-ZB has the strongest sharing electrons which related to the shortest bond length.

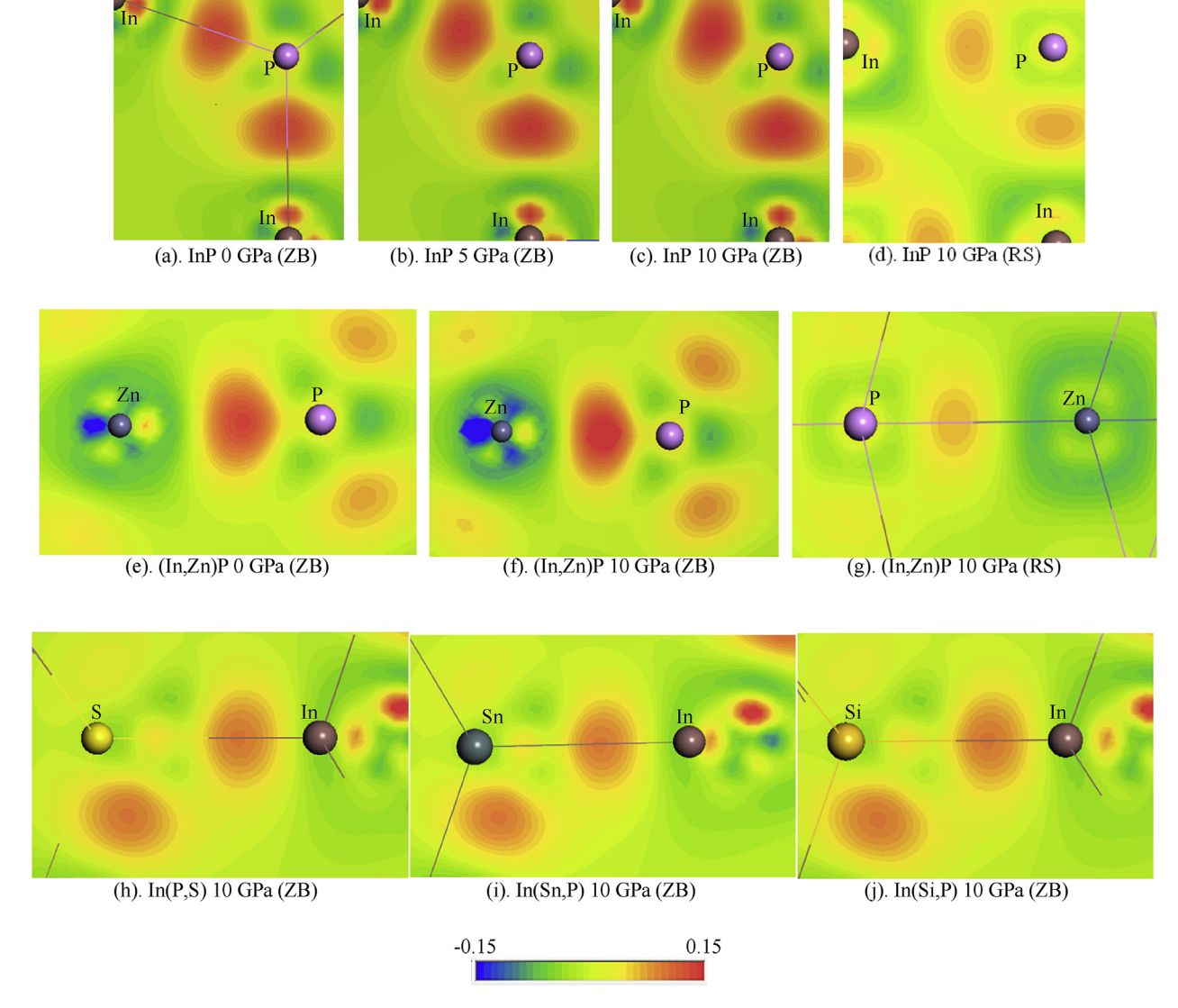


Fig. 4. Electron density difference between two atoms of InP and their alloys under pressure.

**Table 4**Bond lengths between two atoms in the alloys and pure of InP under pressure.

Structure	P (GPa)	Bond ler	Bond length (Å)						
		In-P	Zn-P	In-Si	In-Sn	In-S			
ZB	0	2.525	2.354	2.532	2.657	2.582			
	5	2.474	2.295	2.479	2.602	2.531			
	10	2.435	2.249	2.436	2.563	2.495			
RS	5	2.668	2.542	2.705	2.801	2.708			
	10	2.630	2.505	2.664	2.757	2.671			

### 3.3. Optical properties

The optical properties are also investigated so that photoabsorption of the InP alloys under pressure will be compared and suggested the suitable condition for photo-application. Probability transition states of carriers from valence band to conduction band related to dielectric function, which the external photo energy is translated to the excited energy of intrinsic and extrinsic carriers. Real and imaginary parts of dielectric functions, which are the basic parameters to obtain all optical properties, are presented, and compared with the experiment in range of energies 0.5-6.0 eV [36] as shown in Fig. 5(a). The calculated dielectric functions shifted in low frequency (-x axis) when compared with experiment (dot line) because of the lower pseudogap from calculation with LDA. However, the trends of two graphs are in consistent with experiment [36]. The calculated dielectric functions of (In,Zn)P in Fig. 5(b) are smooth functions more than in InP. At high-pressure (10 GPa), the imaginary part of (Zn,In)P has shifted to the positive frequency (+x axis) which is consistent with previous work [15]. At low frequencies range 0-2 GPa, the imaginary part is dominated as  $\varepsilon_2 > \varepsilon_1$ . The dielectric performance is reduced by the alloying elements due to the reducing of  $\varepsilon_2/\varepsilon_1$  ratio, and it transforms to conductor performance as high frequencies.

Photoabsorption can be obtained from the dielectric function through the Kramers–Kronig relations [37]. Photo absorption in wavelength between 200 and 850 nm (in range of ultraviolet, visible light and infrared) is given in Fig. 6. We found that high-pressure in ZB phase gives unsuitable condition for photoabsorption of InP alloys. Absorption coefficient of the InP alloys in ZB phase decreases under the increasing pressure, while it increases in RS phase. However, the InP alloys had become the non-

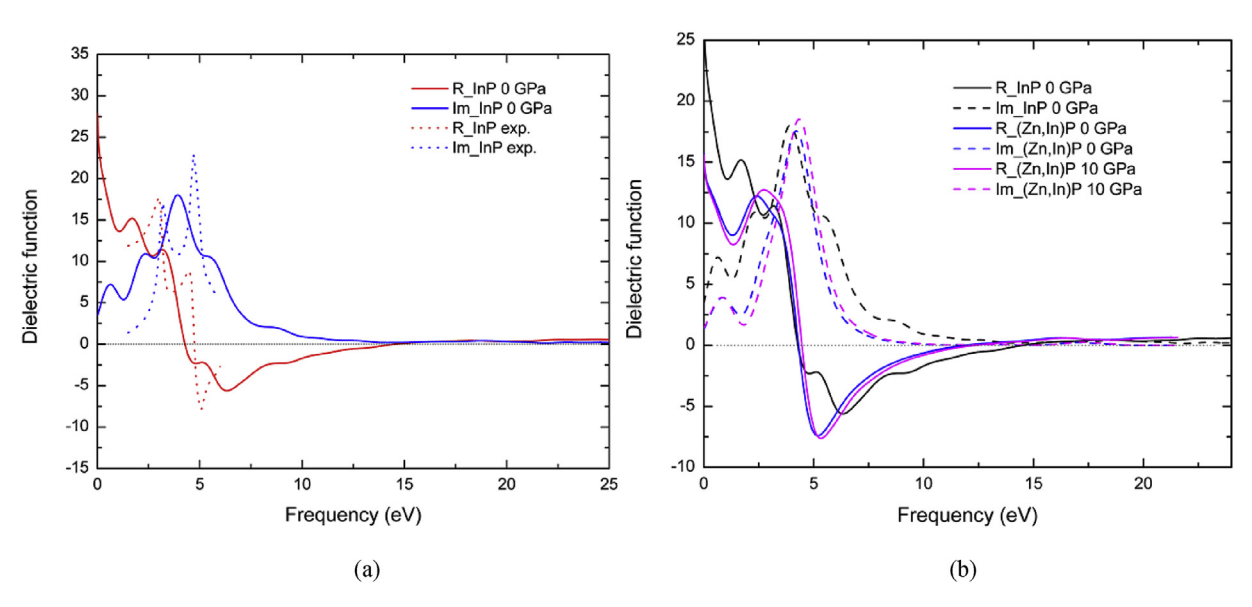


Fig. 5. The calculated dielectric functions in real (R) and imaginary (Im) parts (a) comparison with previous experiment [36] (b) comparison between InP and (In,Zn)P at 0 and 10 GPa.

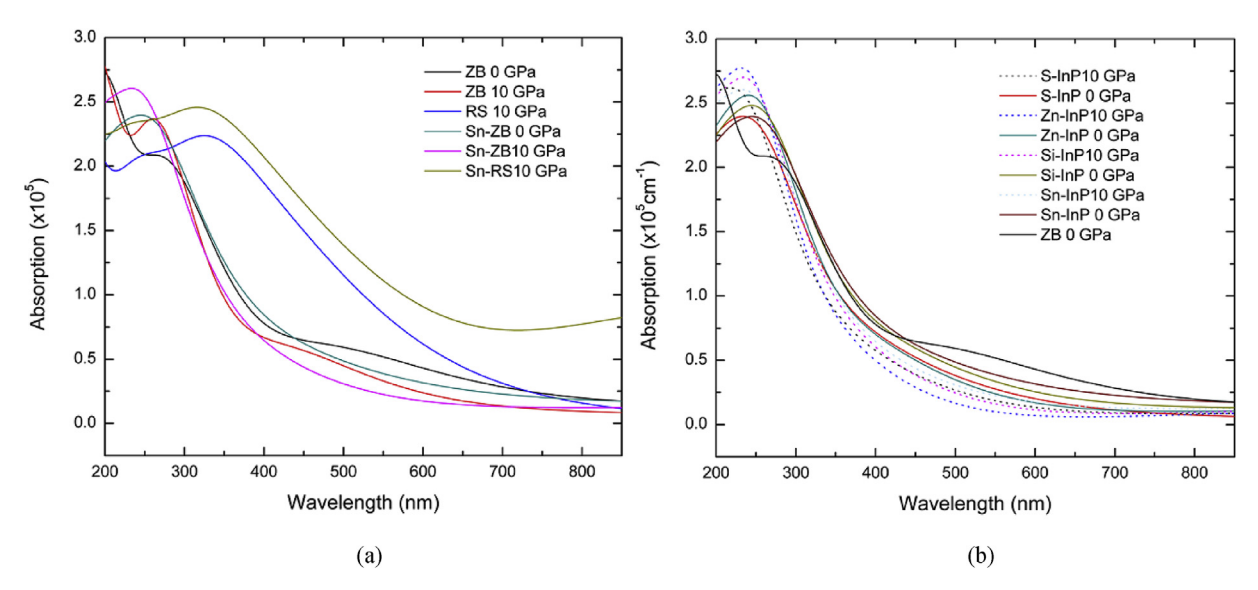


Fig. 6. Photoabsorptions of (a) InP and In(P,Sn) in ZB and RS. (b) (Zn,In)P, In(P,S), In(Si,P), In(Sn,P) and InP in ZB at 0 and 10 GPa.

semiconductor due to the closed band gap. The photoabsorptions generally focus on the semiconductor phase (ZB) that the carrier transition through band gap. In Fig. 6(b), we can see that absorption coefficients of the InP alloys are lower than of pure condition. Order of absorption coefficient of InP-ZB with impurities is Sn>Si>S>Zn, and it decreases at high pressure (10 GPa). Photoabsorptions in ZB are normally reduced under high pressure due to the increasing band gap and the decreasing peaks of EDOSs at VBM and CBM.

### 3.4. Mechanical properties

Elastic constants are calculated to investigate the mechanical properties of the alloying conditions of InP under pressure. The elastic constants  $(c_{ij})$  can provide the hardness, stress and strain in each direction of external forces on a primitive cell of material. The calculated elastic constants of InP with the LDA-CAPZ, GGA-PBE and GGA-PBEsol functionals are compared with the previous

experiment [6] as shown in Table 5. We can see that the LDA-CAPZ result is in good agreement with previous experiment [6], better than PBE and PBEsol. The calculated elastic stiffness constants are satisfied the Born stability criteria in conditions of cubic system (both ZB and RS) [38,39]:  $c_{11} + 2c_{12} > 0$ ,  $c_{44} > 0$ ,  $c_{11} - c_{12} > 0$ .

Bulk modulus (B), Shear modulus (G), Young's modulus (Y) and Poisson's ratio ( $\nu$ ) can be obtained from  $c_{ij}$  based on VRH method

**Table 5**The calculated elastic properties (in GPa unit) by varying functionals compared with experiment results of InP at 0 GPa.

Method	C <sub>11</sub>	C <sub>12</sub>	C44	В	G	Y	е
GGA-PBE	86.8	45.5	42.0	59.3	31.5	55.5	0.344
GGA-PBEsol	93.4	51.6	43.1	65.5	32.2	56.6	0.356
LDA-CAPZ	100.6	55.9	46.2	70.8	34.5	60.7	0.357
Exp. [6]	101	56	45	71	22.5	61	0.360

[32,33]. The upper and lower bounds of the averages B and G in VRH scheme are  $B_V$ ,  $B_R$  and  $G_V$ ,  $G_R$ , respectively. For ZB and RS structures in cubic system [40],

$$\begin{split} B_V &= B_R = (1/3)(c_{11} + 2c_{12}), \\ G_V &= (1/5)(c_{11} - c_{12} + 3c_{44}), \\ G_R &= 5(c_{11} - c_{12})c_{44}/(3c_{11} - 3c_{12} + 4c_{44}). \end{split}$$

The bulk values (B, G, Y and  $\nu$ ) are estimated by VRH approximation:

$$B = (B_V + B_R)/2,$$

$$G = (G_V + G_R)/2,$$

$$Y = 9BG/(3B + G),$$

$$\nu = (3B - 2G)/(6B + 2G).$$

From the calculated B and G moduli, Chen et al. [41] proposed that Vickers hardness of polycrystalline materials can be estimated in terms of  $k = \frac{G}{R}$  and G in the form

$$H_V = 2 \Big( k^2 G \Big) \quad -3.$$

Nevertheless, Tian et al. [42] suggested that it may make the negative hardness for some low hardness materials due to the constant term "-3", so they modified new equation which can always give positive values for low hardness materials. Tian et al.'s correction which used in this work is

$$H_V = 0.92k^{1.137}G^{0.708}$$
.

The elastic parameters are shown in Table 6 that the errors of  $c_{ii}$ calculations are less than 1 GPa. There are satisfied the Born stability criteria in all conditions [38,39]. This indicates that structures of InP alloys are mechanically stable phases in ZB and RS. At ambient pressure, almost of B, Y and S of the InP alloys are smaller than of pure InP, especially the reducing of S. The critical B/G ratio of 1.75 separates type of ductile (>1.75) and brittle (<1.75) materials, which was introduced by Pugh [43]. While, Frantsevich et al. [44] suggested another critical ratio of B/G = 2.67. Therefore, highvalue of the B/G ratio indicates ductility of material. When compare between pure and alloyed conditions at a given pressure, almost  $c_{11}$  are decreased by alloying elements, while  $c_{12}$  are increased. Therefore, the substitutions with Zn, S, Si and Sn can change the properties of InP to ductile material. The value of Y indicates ability of resistance from the external tensile-strength that Yof the alloyed conditions increases in ZB (10 GPa) but it reduces in RS at 10 GPa, when compared with ambient pressure. This supported that RS is high symmetry structure which gave high resistance from the perpendicular forces. The parameters of  $c_{11}$ ,  $c_{12}$  and B in ZB are increased under high-pressure because of the reducing of bond length and primitive cell. High Poisson's ratio (>0.25) [45,46] corresponds to the large deformation of volumetric change and high anisotropy as shown in ZB phase. While, Poisson's ratio of InP allovs in high-symmetry RS phase exhibit small deformation supported the higher isotropy, corresponding to high-symmetry cubic phase. High values of B, G and Y in RS in RS supported the packed atoms in high-symmetry system that it reduces the tangential stress. The B/G ratio in RS is lower than in ZB, indicating that ductility of InP alloys are reduced in RS. The estimated Vickers hardness from Tian et al.'s correction is listed in Table 6. We can see that  $H_{\nu}$  of InP-ZB at ambient condition is 4.99 GPa, which is in good agreement with the experiment result (5.4 GPa) [41]. Tendency of  $H_{\nu}$  indicates that all impurities reduce hardness of pure InP.  $H_{\nu}$ decreases in ZB phase at high pressure (10 GPa) but it increases when transform to RS phase ( $H_v = 11.25$  GPa). The results of Vickers hardness in all compounds supported that RS phase is high symmetry structure because there are increased at the transition pressure of ZB-RS.

### 4. Conclusions

First-principles study on structural, electronic, optical and mechanical properties of Zn, Si, Sn and S substituted in InP supercell in ZB and RS structures are reported. Cohesive energy and enthalpy are observed, and indicated that In site is a preference site of Znalloyed, while a preference site of Sn, Si and S elements in InP is the P site. The possible spontaneous process in experimental growth which is introduced from  $H-H_0$  is (In,Zn) P > In(P,S) > In(Si,P) > In(Sn,P). The lower  $\Delta H$  in RS structure indicates that the spontaneous process of impurity substitution can be occurred in RS more than in ZB. For electronic structure, the porbital is mainly in available states in all compounds. Phase transition from ZB to RS reduces the strain on crystal lattice by the increasing of chemical bond length. The chemical bonding of Zn-P in ZB is the strongest sharing electrons when compared with other compounds, Zn-P>Si-In>Sn-In. For optical properties, the dielectric performance compared from  $\varepsilon_2/\varepsilon_1$  ratio is reduced by the alloying effect, and it transforms to conductor performance at high frequencies. Effect of impurities on ability of photo-absorption in range of visible light is Sn>Si>S>Zn, and it reduces as the pressure increasing. Mechanical stability of InP alloys was observed, and satisfied the Born stability criteria. The impurities reduce Shear modulus of pure InP. Poisson's ratio of InP alloys in RS exhibit small deformation and high isotropy, corresponding to high-symmetry cubic phase. High values of B, G and Y in RS supported atomic structure in RS that packed in high-symmetry system. B/G ratio

 $\textbf{Table 6} \\ \textbf{Elastic parameters in a unit GPa (except} \textit{e}) \text{ of InP and their alloys in ZB and RS structures.}$ 

Structure	condition	C <sub>11</sub>	c <sub>12</sub>	c <sub>44</sub>	В	G	Y	$\varepsilon$	B/G	$H_V$
ZB	InP	100.6	55.9	46.2	70.8	34.5	60.7	0.36	2.05	4.99
0 GPa	(In,Zn)P	87.6	63.0	30.6	71.2	21.2	57.1	0.42	3.36	2.02
	In(P,S)	86.7	51.6	32.8	63.3	25.5	46.3	0.37	2.48	3.24
	In(Si,P)	82.3	60.4	23.8	67.7	17.4	56.1	0.42	3.89	1.48
	In(Sn,P)	75.2	59.6	16.7	64.8	12.3	56.6	0.44	5.27	0.82
10 GPa	InP	139.1	100.5	44.4	113.4	31.8	54.9	0.42	3.56	2.51
	(In,Zn)P	125.2	108.1	23.8	113.8	15.6	103.3	0.46	7.29	0.67
	In(P,S)	124.3	99.3	28.7	107.6	20.6	93.9	0.44	5.22	1.20
	In(Si,P)	121.4	106.8	19.6	111.7	13.2	102.9	0.47	8.46	0.50
	In(Sn,P)	114.0	105.1	10.1	108.0	7.3	103.2	0.48	14.79	0.18
RS	InP	269.4	64.2	66.2	132.6	79.0	244.7	0.19	1.68	11.25
10 GPa	(In,Zn)P	264.2	76.1	24.1	138.8	43.2	110.0	0.22	3.21	3.51
	In(P,S)	251.2	74.1	30.0	133.1	47.1	101.7	0.23	2.83	4.32
	In(Si,P)	229.6	78.2	29.0	128.7	43.1	99.9	0.25	2.99	3.81
	In(Sn,P)	224.2	73.1	23.2	123.5	38.1	103.6	0.36	3.24	3.18

indicates that ductility of all alloys in RS is reduced, when compared with ZB. The ductility of InP is induced by the alloying effect due to the B/G ratio increasing. High value of Vickers hardness in RS phase of all compounds supported that RS is high symmetry structure.

### Acknowledgments

P. Pluengphon would like to thank the financial support from Thailand Research Fund ID code TRG5880006, and Faculty of Science and Technology, Huachiew Chalermprakiet University. This work has been partially supported by National Research Council of Thailand. Computing facilities have been supported by Super SCI-II research grant, Faculty of Science and Ratchadaphiseksomphot Endowment Fund of Chulalongkorn University (CU-59-039-AM).

### References

- [1] G.J. Ackland, Rep. Prog. Phys. 64 (2001) 483.
- [2] I. Vurgaftman, J.R. Meyer, L.R. Ram-Mohan, J. Appl. Phys. 89 (2001) 5815.
- [3] N. Bouarissa, Phys. B 406 (2011) 2583.
- [4] P.L. Souza, P.R. Ribas, J.V. Bellini, W.M. Mendes, J. Appl. Phys. 79 (1996) 3482.
- [5] C.S. Menoni, I.L. Spain, Phys. Rev. B 35 (1987) 7520.
- [6] D.N. Nichols, D.S. Rimai, R.J. Sladek, Sol. Stat. Comm. 36 (8) (1980) 667.
- [7] A. Mujica, R.J. Needs, Phys. Rev. B 55 (1997) 9659.
- [8] H. Xue, F. Tang, W. Lu, Y. Feng, Z. Wang, Y. Wang, Comput. Mater. Sci. 67 (2013) 21.
- [9] P. Pluengphon, T. Bovornratanaraks, Sol. Stat. Comm. 218 (2015) 1.
- [10] M. Durandurdu, D.A. Drabold, Phys. Rev. B Condens. Matter 66 (2002) 045209.
- [11] P. Pluengphon, T. Bovornratanaraks, S. Vannarat, U. Pinsook, Solid State Commun. 195 (2014) 26.
- [12] Y. Zhao, H. Hou, Y. Zhao, P. Han, J. Alloys Compd. 640 (2015) 233.
- [13] J. Long, C. Shu, L. Yang, M. Yang, J. Alloys Compd. 644 (2015) 638.
- [14] Y. Xu, C. Chen, S. Wang, X. Sun, J. Alloys Compd. 669 (2016) 101.
- [15] N. Bouarissa, Solid State Electron. 44 (2000) 2193.
- [16] N. Bouarissa, Mater. Chem. Phys. 65 (2000) 107.

- [17] N. Bouarissa, Infrared Phys. Technol. 40 (1999) 117.
- [18] Y. Moon, S. Si, E. Yoon, S.J. Kim, J. Appl. Phys. 83 (1998) 2261.
- [19] E.F. Schubert, C.J. Pinzone, M. Geva, Appl. Phys. Lett. 67 (5) (1995) 700.
  [20] J. Decobert, D. Herrati, V. Colson, D. Leclerc, L. Goldstein, J. Cryst. Growth 248
- (2003) 390.
- [21] S.B. Youssef, Phys. A 235 (1997) 334.
- [22] H. Hu, X. Wu, R. Wang, Z. Jia, W. Li, Q. Liu, J. Alloys Compd. 666 (2016) 185.
- [23] Y. Hu, S. Shang, Y. Wang, et al., J. Alloys Compd. 671 (2016) 267.
- [24] M.C. Payne, M.P. Teter, D.C. Allan, T.A. Arias, D. Joannopoulos, Rev. Mod. Phys. 64 (1992) 1045.
- [25] M.D. Segall, P.L.D. Lindan, M.J. Probert, C.J. Pickard, P.J. Hasnip, S.J. Clark, M.C. Payne, J. Phys. Condens. Matter 14 (2002) 2717.
- [26] J.P. Perdew, J.A. Chevary, S.H. Vosko, K.A. Jackson, M.R. Pederson, D.J. Singh, C. Fiolhais, Phys. Rev. B 46 (1992) 6671.
- [27] J.P. Perdew, K. Burke, M. Ernzerhof, Phys. Rev. Lett. 77 (1996) 3865.
- [28] D. Vanderbilt, Phys. Rev. B 41 (1990) 7892.
- [29] H.J. Monkhorst, J.D. Pack, Phys. Rev. B 13 (1976) 5188.
- [30] B.G. Pfommer, M. Cote, S.G. Louie, M.L. Cohen, J. Comput. Phys. 131 (1997) 233.
- [31] R.P. Feynman, Phys. Rev. 56 (4) (1939) 340.
- [32] R. Hill, Proc. Phys. Soc. A 65 (1952) 349.
- [33] G.V. Sinko, N.A. Smirnov, J. Phys. Condens. Matter 14 (2002) 6989.
- [34] L. Li, Q. Gao, G. Lei, H. Xie, J. Deng, Xian-Ru Hu, J. Phys. Chem. Solids 94 (2016) 30–36.
- [35] P. Pluengphon, T. Bovornratanaraks, S. Vannarat, U. Pinsook, J. Phys. Condens. Matter 24 (2012) 095802.
- [36] D.E. Aspnes, A.A. Studna, Phys. Rev. B 27 (1983) 985.
- [37] R.F. Egerton, Electron Energy-loss Spectroscopy in the Electron Microscope, second ed., Plenum Press, New York, 1996. ISBN 0-306-45223-5.
- [38] B.B. Karki, G.J. Ackland, J. Crain, J. Phys. Condens. Matter 9 (1997) 8579.
- [39] F. Mouhat, F.X. Coudert, Phys. Rev. B 90 (2014) 224104.
- [40] X. Zhang, W. Jiang, J. Alloys Compd. 663 (2016) 565.
- [41] X.Q. Chen, H. Niu, D. Li, Y. Li, Intermetallics 19 (2011) 1275.
- [42] Y.J. Tian, B. Xu, Z.S. Zhao, Int. J. Refract. Met. Hard Mater. 33 (2012) 93.
- [43] S.F. Pugh, Philos. Mag. 45 (1953) 833.
- [44] I.N. Frantsevich, F.F. Voronov, S.A. Bokuta, Elastic Constants and Elastic Moduli for Metals and Insulators Handbook, Naukova Dumka, Kiev, 1983.
- [45] S. Aydin, M. Simsek, J. Alloys Compd. 509 (2011) 5219.
- [46] C. Li, K. Zhang, J. Ru, J. Alloys Compd. 647 (2015) 573.





(High Pressure Phases of InP Calculated Using Density Functional Theory) Prayoonsak Pluengphon<sup>a,\*</sup>, Thiti Bovornratanaraks<sup>b,c</sup>

<sup>a</sup>Division of Physical Science, Faculty of Science and Technology, Huachiew Chalermprakiet University, Samutprakarn, Thailand

°ThEP Center, CHE, 328 Si-Ayuttaya Road, Bangkok , Thailand \*Corresponding Author E-mail: pprayoonsak@hotmail.com

bExtreme Conditions Physics Research Laboratory, Department of Physics, Faculty of Science, Chulalongkorn University, Bangkok , Thailand

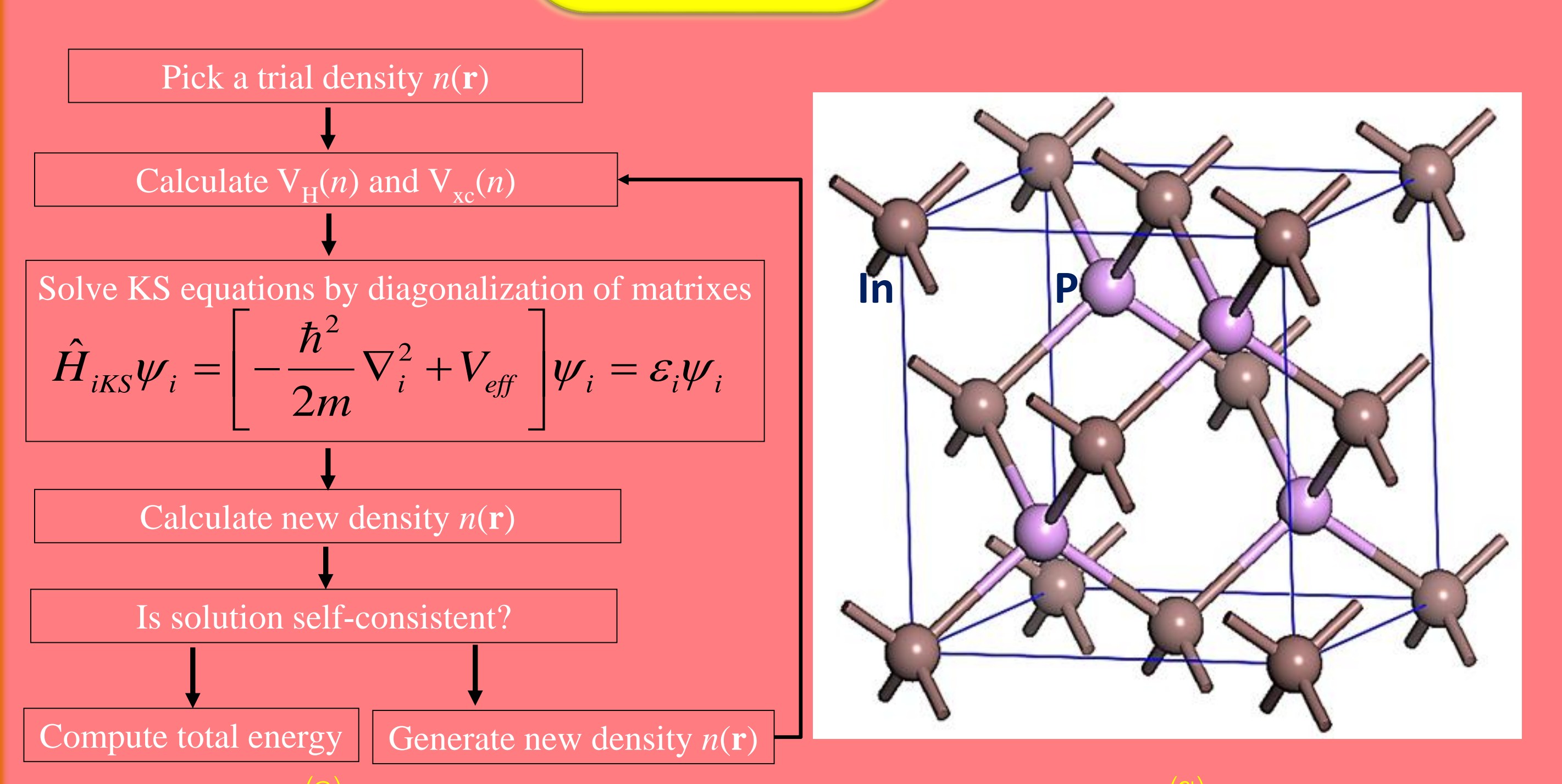


### บทคัดย่อ

ในศาสตร์ฟิสิกส์ของแข็งนั้น โครงสร้างที่เสถียรและสมบัติทางกายภาพของของแข็งสามารถเปลี่ยนแปลงโดยผลกระทบจากความดันสูงในระดับจิกกะปาสคาล สารประกอบแบบสองธาตุในกลุ่ม III-V มีการศึกษาอย่างแพร่หลายเพื่อที่จะใช้ในการ ประยุกต์ที่หลากหลายเกี่ยวกับการแปรค่าได้ของความต้านทานของสารกึ่งตัวนำโดยเฉพาะไดโอดเปล่งแสง อุปกรณ์อิเล็กทรอนิกส์ และเซลล์สุริยะแบบหลายชั้น ในงานวิจัยนี้ สนใจศึกษาสมบัติภายใต้ความดันของสารอินเดียมฟอสไฟด์ซึ่งเป็นสารประกอบแบบ สองธาตุในกลุ่มหมู่ III-V สมบัติทางเทอร์โมไดนามิกส์ของสารควบแน่นสามารถคำนวณโดยใช้ทฤษฎีฟังก์ชั้นนอลความหนาแน่น โครงสร้างเสถียรในแต่ละช่วงความดันทำการเปรียบเทียบโดยใช้ค่าเอนทัลปีที่ต่ำที่สุด พลังงานอิสระของโครงสร้างที่สนใจศึกษาจะ ได้รับจากผลการแก้สมการโคห์นชามซึ่งมีพื้นฐานของทฤษฎีฟังก์ชันนอลความหนาแน่น ผลการวิจัยพบว่าผลของการคำนวณที่สภาวะความดันปกติและการเปลี่ยนเฟสครั้งแรกสอดคล้องกับผลการทดลองที่มีอยู่ในงานวิจัยก่อนหน้า อย่างไรก็ตามงานวิจัยนี้ขยาย ผลจากงานวิจัยอื่นๆ ก่อนหน้านี้ด้วย ขนาดของปริมาตรหน่วยเซลล์ลดลงภายใต้ความดันที่เพิ่มขึ้น ความเป็นสารกึ่งตัวนำของสารได้กลายเป็นกึ่งโลหะเนื่องจากการเปลี่ยนเฟส

### บทน้า

สารกึ่งตัวนำประกอบแบบสองธาตุในกลุ่มหมู่ III-V มีการศึกษาอย่างแพร่หลายเพื่อที่จะใช้ในการประยุกต์ที่ หลากหลายเกี่ยวกับการแปรค่าได้ของความต้านทานของสารกึ่งตัวนำโดยเฉพาะไดโอดเปล่งแสง (light emitting diode, LED) ้อุปกรณ์อิเล็กทรอนิกส์ และเซลล์สุริยะแบบหลายชั้น หนึ่งในสารประกอบแบบสองธาตุในกลุ่มหมู่ III-V คือ อินเดียมฟอสไฟด์ (Indium Phosphide, InP) (Nichols, Rimai, & Sladek, 1980) มีการใช้สารนี้อย่างแพร่หลายในการนำมาทำเป็นฐานของ ฟิล์มบางในโครงสร้างของเซลล์สุริยะแบบหลายชั้น สารอินเดียมฟอสไฟด์ที่ความดันบรรยากาศมีโครงสร้างแบบซิงค์เบลน (zinc blende) ซึ่งมีกลุ่มปริภูมิ (space group) คือ *F-43m* (Bouarissa, 2011) โครงสร้างแบบซิงค์เบลนเป็นหนึ่งในโครงสร้างแบบ ลูกบาศก์ (cubic structure) คล้ายกับสารอื่นในกลุ่มหมู่เดียวกัน ในการทดลองอัดความดันของสารด้วยเครื่องอัดแบบแท่ง เพชร (diamond anvil cell, DAC) แล้วทดสอบโครงสร้างผลึกด้วยการศึกษารูปแบบการกระเจิงของรังสีเอ็กซ์เมื่อเพิ่มความ ์ ดันพบว่าสารมีการเปลี่ยนแปลงโครงสร้างมีลำดับ คือ *F-43m-->Fm-3m-->Cmcm-->Immm--> Pm-3m* ที่ความดัน 5.6 ี่ 11.0 50.0 และ 102.0 จิกกะปาสคาล (GPa) ตามลำดับ (Ackland,2001) นอกจากการเข้าถึงองค์ความรู้ที่มีอยู่ในธรรมชาติ ้ด้วยการทำการทดลองแล้ว ความก้าวหน้าในด้านทฤษฎีก็สามารถทำให้ทราบถึงโครงสร้างของสารภายใต้ความดันได้อีกด้วย ิทฤษฎีที่นิยมใช้ในการทำนายโครงสร้างของสาร คือ ทฤษฎีฟังก์ชันนอลความหนาแน่น (density functional theory, DFT) (Payne, Teter, Allan, Arias, & Joannopoulos, 1992) ซึ่งสามารถทำนายลำดับการเปลี่ยนเฟสของสารหลายชนิดได้อย่าง ้ถูกต้อง และทำให้อธิบายธรรมชาติของสสารหรือผลการทดลองได้ดียิ่งขึ้นอีกด้วย ทฤษฎีจึงเป็นสิ่งเติมเต็มให้องค์ความรู้นั้น ้เชื่อมโยงกันได้ดียิ่งขึ้นตลอดจนตอบคำถามหรือข้อสงสัยที่ค้นพบจากการทดลองได้อีกด้วย จากที่กล่าวมาได้มีการศึกษา ิโครงสร้างภายใต้ความดันสูงอยู่บ้าง อย่างไรก็ตามองค์ความรู้ที่มียังไม่สมบูรณ์และสามารถศึกษาต่อยอดเพิ่มเติมได้อีก ดังนั้นใน งานวิจัยนี้จึงสนใจศึกษาสมบัติภายใต้ความดันของสารอินเดียมฟอสไฟด์ซึ่งเป็นสารประกอบแบบสองธาตุในกลุ่มหมู่ III-V



ภาพที่ 1 (ก) แผนภาพการค้านวณหาค่าพลังงาน (ข) หน่วยเซลล์ของสารอิน

งานวิจัยนี้ทำการศึกษาโครงสร้างของสารอินเดียมฟอสไฟด์โดยใช้ทฤษฎีฟังก์ชันนอลความหนาแน่นคำนวณผ่าน สมการโคห์นชาม (Kohn-Sham equations) หลักการเบื้องต้นของทฤษฎีฟังก์ชันนอลความหนาแน่นเริ่มจากทฤษฎีบทของ โฮเฮ็นเบิร์กและโคห์น (Hohenberg-Kohn theorems) ซึ่งกล่าวโดยสรุปอย่างง่ายว่าปริมาณต่างๆที่สามารถตรวจวัดได้เป็น ฟังก์ชันนอลของความหนาแน่นของอิเล็กตรอน และกล่าวว่าจะมีความหนาแน่นของอิเล็กตรอนรูปแบบเดียวที่ทำให้เกิด ระดับพลังงานต่ำสุดในสถานะพื้นของระบบ จากทฤษฎีบทดังกล่าวและการใช้วิธีวาริเอชันนอล (variational method) (Payne et al., 1992) จะได้สมการคล้ายสมการของชโรดิงเจอร์ ดังแสดงในภาพที่ 1(ก)

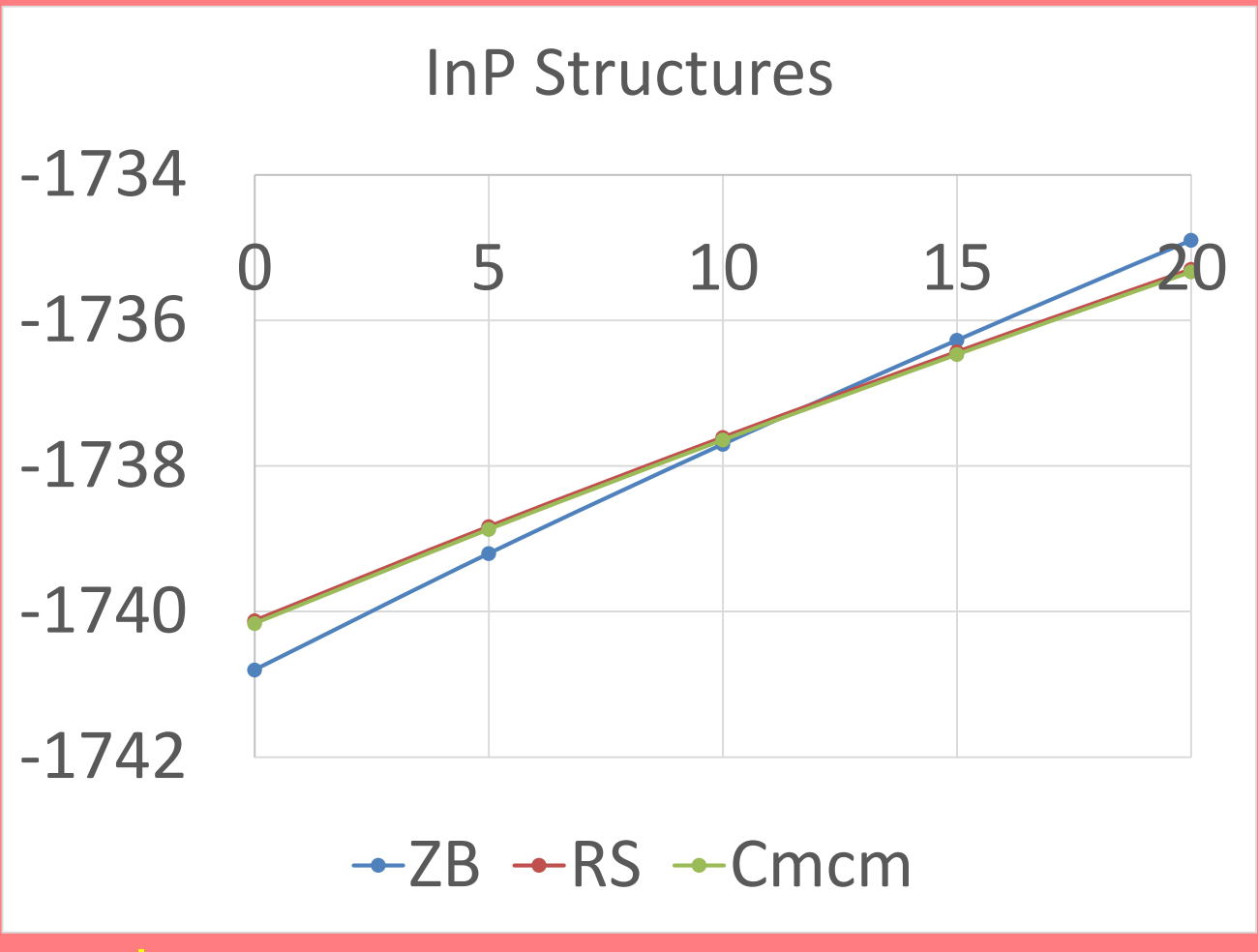
ในงานวิจัยนี้ศึกษาสมบัติภายใต้ความดันของสารอินเดียมฟอสไฟด์ซึ่งเป็นสารประกอบแบบสองธาตุในกลุ่มหมู่ III-V ผลการวิจัยพบว่าผลของการคำนวณที่สภาวะความดันปกติและการเปลี่ยนเฟสครั้งแรกสอดคล้องกับผลการทดลองที่มี อยู่ในงานวิจัยก่อนหน้า อย่างไรก็ตามงานวิจัยนี้ขยายผลจากงานวิจัยอื่นๆ ก่อนหน้านี้ด้วย ขนาดของปริมาตรหน่วยเซลล์ ลดลงภายใต้ความดันที่เพิ่มขึ้น ความเป็นสารกึ่งตัวนำของสารได้กลายเป็นกึ่งโลหะเนื่องจากการเปลี่ยนเฟส ภายใต้ความดัน ้ที่สูงขึ้นค่ามอดูลัสเชิงปริมาตรมีค่าเพิ่มขึ้นเนื่องจากได้รับอิทธิพลจากแรงกดแบบทุกทิศทาง ส่วนค่ามอดูลัสเฉือนจะมีค่า ้สูงขึ้นมากในโครงสร้าง RS เนื่องจากโครงสร้างแบบลูกบาศก์มีสมมาตรสูงกว่าโครงสร้างแรกที่ความดันปกติ ทำนองเดียวกัน ความสามารถในการยืดหดตามความยาวของสารมีค่าสูงในโครงสร้างที่สอง ทั้งนี้เพราะอะตอมมีการจัดเรียงในรูปแบบที่ หนาแน่นมากขึ้นจึงทนทานต่อผลของแรงภายนอกได้ดีนั่นเอง ข้อมูลนี้สามารถยืนกันได้เนื่องจากเมื่อเราพิจารณาการสร้าง พันธะโดยดูจากการกระจายของอิเล็กตรอนดังภาพจะเห็นว่าในโครงสร้างที่สองมีการร่วมใช้อิเล็กตรอนมากกว่าโครงสร้าง แรก เมื่อความดันเพิ่มขึ้นอิเล็กตรอนจะกองอยู่ตรงกลางระหว่างอะตอมทั้งสองประเภทมากขึ้น ทำให้พันธะเคมีมีความ แข็งแรงมากขึ้น

## ผลการวิจัย

ในการตรวจสอบความถูกต้องการผลการคำนวณจะทำการเปรียบเทียบผลที่คำนวณได้เทียบกับผลการทดลองใน ส่วนที่มีผลอยู่ในงานวิจัยก่อนหน้า ซึ่งค่าพารามิเตอร์พื้นฐานที่ความดันปกติ มีผลเปรียบเทียบดังนี้

**ตารางที่ 1** แสดงการเปรียบเทียบผลการคำนวณกับผลการทดลอง

พารามิเตอร์/วิธีการ	การทดลอง (Nichols et al., 1980)	คำนวณด้วย GGA-PBE (งานนี้)	คำนวณด้วย LDA-CAPZ (งานนี้)
ขนาดของหน่วยเซลล์ (Å)	5.856	5.968	5.832
มอดูลัสเชิงปริมาตร (GPa)	71.1	59.3	71.8



มอดูลัสเฉือน มอดูลัสของยัง โครงสร้าง มอดูลัสเชิง ปริมาตร ZB 0 GPa 71.8 34.2 60.7 ZB 5 GPa 93.9 33.3 58.7

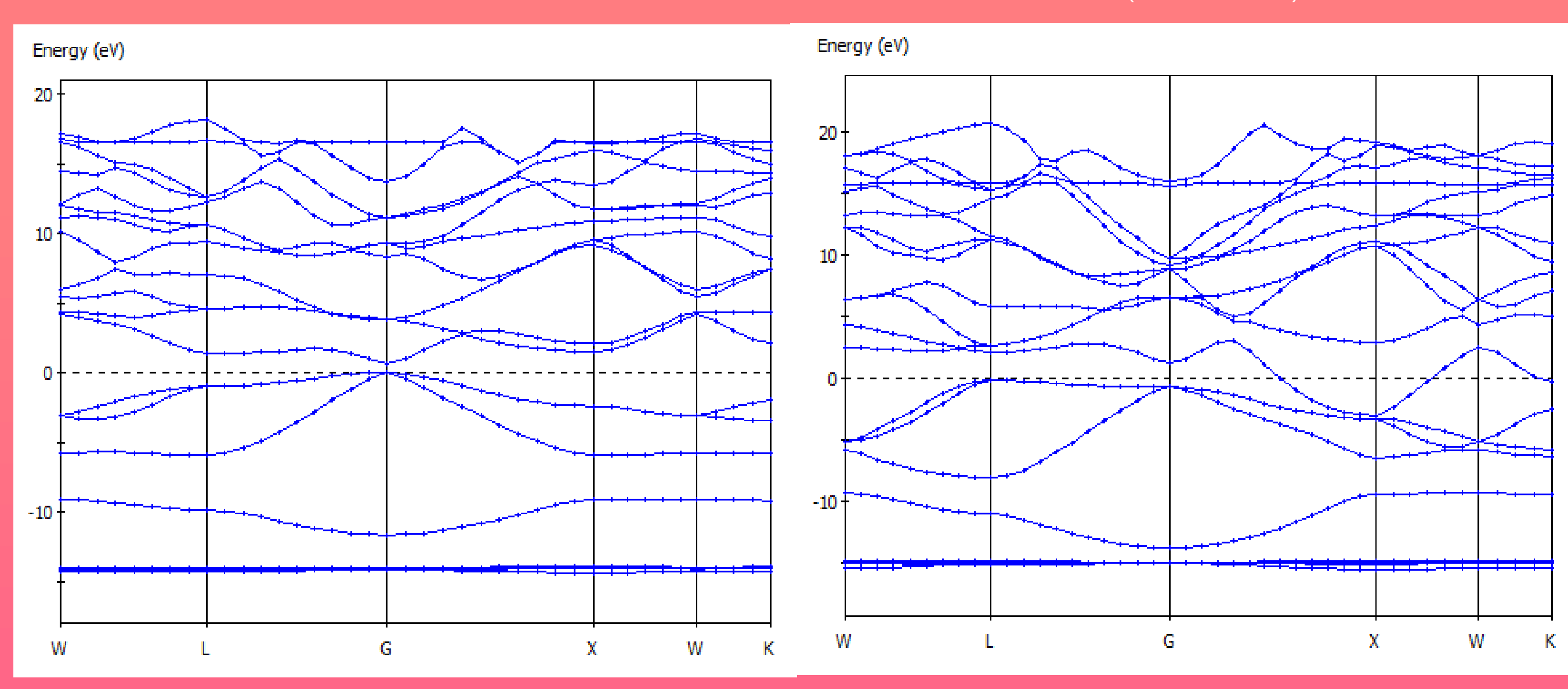
132.6

79.0

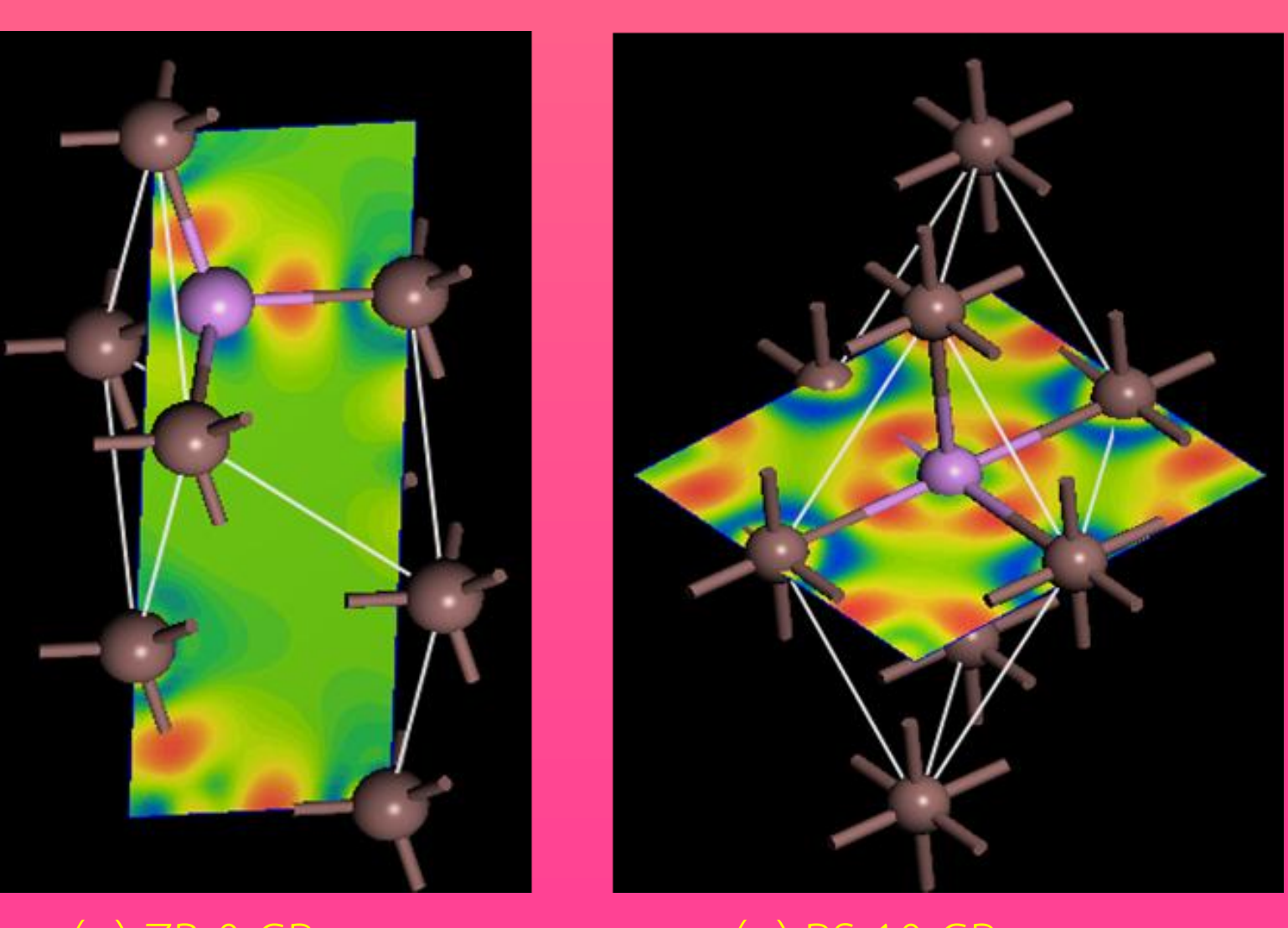
244.7

ทำการเปรียบเทียบผลการคำนวณทั้ง 3 โครงสร้าง คือ แบบซิงค์เบลน (ZB) แบบหินเกลือ (RS) และ แบบออร์โทรอมบิค (*Cmcm*) ตามลำดับ ในภาพที่ 2 พบว่าที่ความดันช่วงต่ำสุด คือ 0-12 GPa สารอินเดียมฟอสไฟด์มีโครงสร้างแบบ ZB ตามผล การทดลอง และเมื่อเพิ่มความดันมากกว่า 12 GPa สารจะเปลี่ยนโครงสร้างเป็นแบบลูกบาศก์ (RS) สำหรับโครงสร้าง Cmcm นั้น เราพบว่าจะมีเส้นพลังงานทับกับโครงสร้างแบบ RS พอดี ทั้งนี้เนื่องจากเมื่อทำการ geometry optimization โครงสร้าง Cmcm จะได้โครงสร้างพลังงานต่ำลู่เข้าหา RS นั่นเอง เมื่อความดันเพิ่มขึ้นพบว่าช่องว่างพลังงานมีค่าเพิ่มขึ้นตามความดันเมื่อ อยู่ในโครงสร้างแรก แต่เมื่อสารเปลี่ยนโครงสร้างเป็นโครงสร้างแบบโซเดียมคลอไรด์ที่ 10 GPa พบว่าช่องว่างพลังงานหายไป ้นั่นคือ แถบพลังงานนำและแถบพลังงานเวเลนซ์เชื่อมติดกัน เหตุการณ์นี้สื่อให้เห็นว่าเมื่อสารอินเดียมฟอสไฟด์เปลี่ยน โครงสร้างไปจะทำให้คุณสมบัติความเป็นสารกึ่งตัวนำหายไปด้วยโดยอินเดียมฟอสไฟด์จะกลายเป็นสารที่ไม่ใช่สารกึ่งตัวนำอีก ้ต่อไป โดยทั่วไปแล้วสารกึ่งตัวนำเมื่อถูกอัดด้วยความดันสูงสารจะกลายเป็นตัวนำ สำหรับในภาพพบว่าแถบพลังงานเวเลนซ์มี ส่วนที่ยื่นขึ้นมาซ้อนกับแถบพลังงานนำในบางส่วนเท่านั้นซึ่งเป็นลักษณะของสารกึ่งโลหะ (semimetal)

RS 10 GPa



ภาพที่ 3 แสดงโครงสร้างแถบพลังงานในโครงสร้าง (ก) แบบซิงค์เบล<sup>ิ</sup>นที่ 0 GPa (ข) แบบโซเดียมคลอไรด์ที่ 10 GPa



ในบริเวณต่างๆของทั้งสองโครงสร้าง

เมื่อเราพิจารณาการสร้างพันธะโดยดุจากการกระจาย ของอิเล็กตรอนดังภาพที่ 4 จะเห็นว่าในโครงสร้างที่ สองมีการร่วมใช้อิเล็กตรอนมากกว่าโครงสร้างแรก สังเกตจากบริเวณที่มีสีแดงซึ่งบ่งชี้ถึงบริเวณที่มีความ หนาแน่นในการพบเวเลนซ์อิเล็กตรอนสูง เมื่อความ ดันเพิ่มขึ้นอิเล็กตรอนจะกองอยู่ตรงกลางระหว่าง อะตอมทั้งสองประเภทมากขึ้น ทำให้พันธะเคมีมี ความเป็นพันธะโควาเลนซ์มากขึ้นและแข็งแรงขึ้น นั่นเอง

รุ่นใหม่ สกว. ปี 2558 รหัสทุน TRG588000*6* 



# Phase Stability and Mechanical Properties of In(P,S) under Pressure: First-Principles Calculation

Prayoonsak Pluengphon<sup>a,\*</sup>, Thiti Bovornratanaraks<sup>b,c</sup>



<sup>a</sup>Division of Physical Science, Faculty of Science and Technology, Huachiew Chalermprakiet University, Samutprakarn, Thailand

<sup>b</sup>Extreme Conditions Physics Research Laboratory, Department of Physics, Faculty of Science, Chulalongkorn University, Bangkok, Thailand

<sup>c</sup>The Center, CHE, 328 Si-Ayuttaya Road, Bangkok, Thailand

\*Corresponding Author E-mail: pprayoonsak@hotmail.com

### **Abstract**

A first-principles calculation based on density functional theory (DFT) was performed for studying high-pressure properties of In(P,S). For calculation method, the concentration of impurity sulfur atom (S) was studied at 6.25% into super cell size 2x2x2 of InP, which called In(P,S). Phase stability and mechanical properties of InP and In(P,S) were investigated up to 10 GPa, and compared between zinc blend and NaCl-like structures. The enthalpy change, between dope-S and undope, and elastic constant under pressure were compared. It was found that the enthalpy change decreases when pressure increasing. All of the elastic constants calculated from DFT with LDA functional satisfy the Born stability criteria that is the requirements for mechanical stability. Bulk modulus and ductility of InP are increased by adding S atom and pressure.

### Introduction

Alloys and compounds of III-V binary semiconductors are great of interest for developing the electronic devices such as light emitting diodes, optoelectronic devices and photovoltaic materials; especially the solar cell efficiency highly depends on the electronic and optical properties of semiconducting materials in multilayer films. Indium Phosphide (InP) is one of the III-V binary semiconductors which widely used as a substrate for epitaxial growth applied in photovoltaic multilayers. Doping of InP have intensively studied in many applications because electronic properties respond significantly. In this issue, the theoretical studies about elastic constants and density of states of the doped binary alloys are presented.

### **Calculation Details**

In DFT calculation, the solution of ground state properties were evaluated from the Kohn-Sham equations, the eigenvalues and eigenstates (Kohn-Sham orbitals) are solved by using diagonalization of matrixes as shown in Figure 1(a) [1, 2]. In InP super cells, the impurity sulfur atom (S) was replaced on a P site at 6.25% into super cell of InP as shown in Fig 1(b).

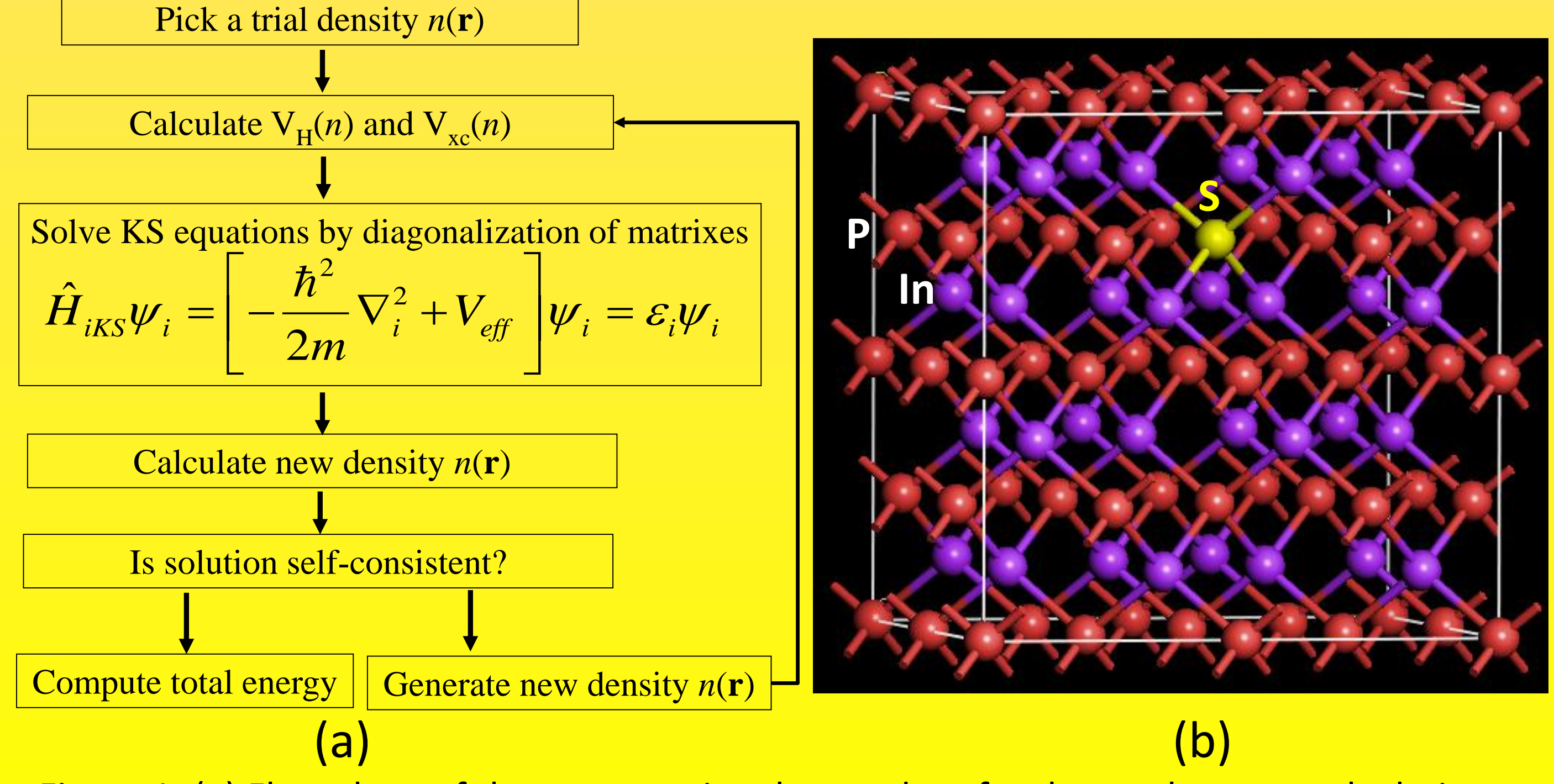


Figure 1: (a) Flow chart of the computational procedure for the total energy calculation [1]. (b) Super cell of InP in ZB phase was substituted by a S atom at P site.

Formation enthalpy and free energies difference at 0 GPa were analyzed as shown in table 1. Formation enthalpy per atom  $(H_f)$  of compounds such as  $In_{1-x}M_xP$  can be calculated in from

$$H_f = \frac{1}{2} H_{total} \left( \text{In}_{1-x} M_x P \right) - \frac{1}{2} \left[ (1-x) H_{solid} \left( \text{In} \right) + (x) H_{solid} \left( M \right) + H_{solid} \left( P \right) \right]$$

Where  $H_{total}$  is the enthalpy of  $In_{1-x}M_xP$  compound, and  $H_{solid}$  is enthalpy of  $In_{1-x}M_xP$  and P in bulk. Formation enthalpy is used to compare ability for adding M atom in InP lattice, while free energies difference will show ability of possible process to fabricating the doped compounds.

### Conclusions

- -Formation enthalpy and free energies difference of S-doped reduce from InP.
- -Peaks of EDOSs of In(P,S) are flatted under pressure increasing.
- -The elastic constants of super cells satisfy the Born stability criteria that is the requirements for mechanical stability.
- -S-doped on P site reduces elastic constants of InP, but it increases under high-pressure.

# Acknowledgments

P. Pluengphon would like to acknowledge the research funding from Thailand Research Fund (TRF) ID code: TRG5880006, and Faculty of Science and Technology, Huachiew Chalermprakiet University.

### **Results and Discussion**

In table 1, it was found that formation enthalpy and free energies difference of S-doped are reduced when compare with the undoped condition.  $G-G_0$  of In(P,S) in ZB phase reduces under high-pressure as shown in table 2. However,  $G-G_0$  is increased when Zb transition to RS phase. Peaks of EDOSs of In(P,S) are flatted under pressure increasing as shown in figure 2.

Table 1: Formation enthalpy and free energies difference of doped and undoped InP at 0 GPa.

compound	H <sub>total</sub>	$H_{solid}$	H <sub>f</sub>	G-G <sub>0</sub>
Undope	-870.40	-866.11	-4.29	0.00
In(P,S)	-876.51	-872.34	-4.17	-6.12
In(Sn,P)	-865.02	-860.95	-4.07	5.38

Table 2: Free energies difference of doped and undoped InP under high pressure.

Phase	Р	$G_{o}$	G-G <sub>0</sub>
		Undope	In(P,S)
ZB	0	-870.40	-6.12
	5	-869.60	-6.10
	10	-868.84	-6.09
RS	5	-869.42	-6.28
	10	-868.80	-6.28

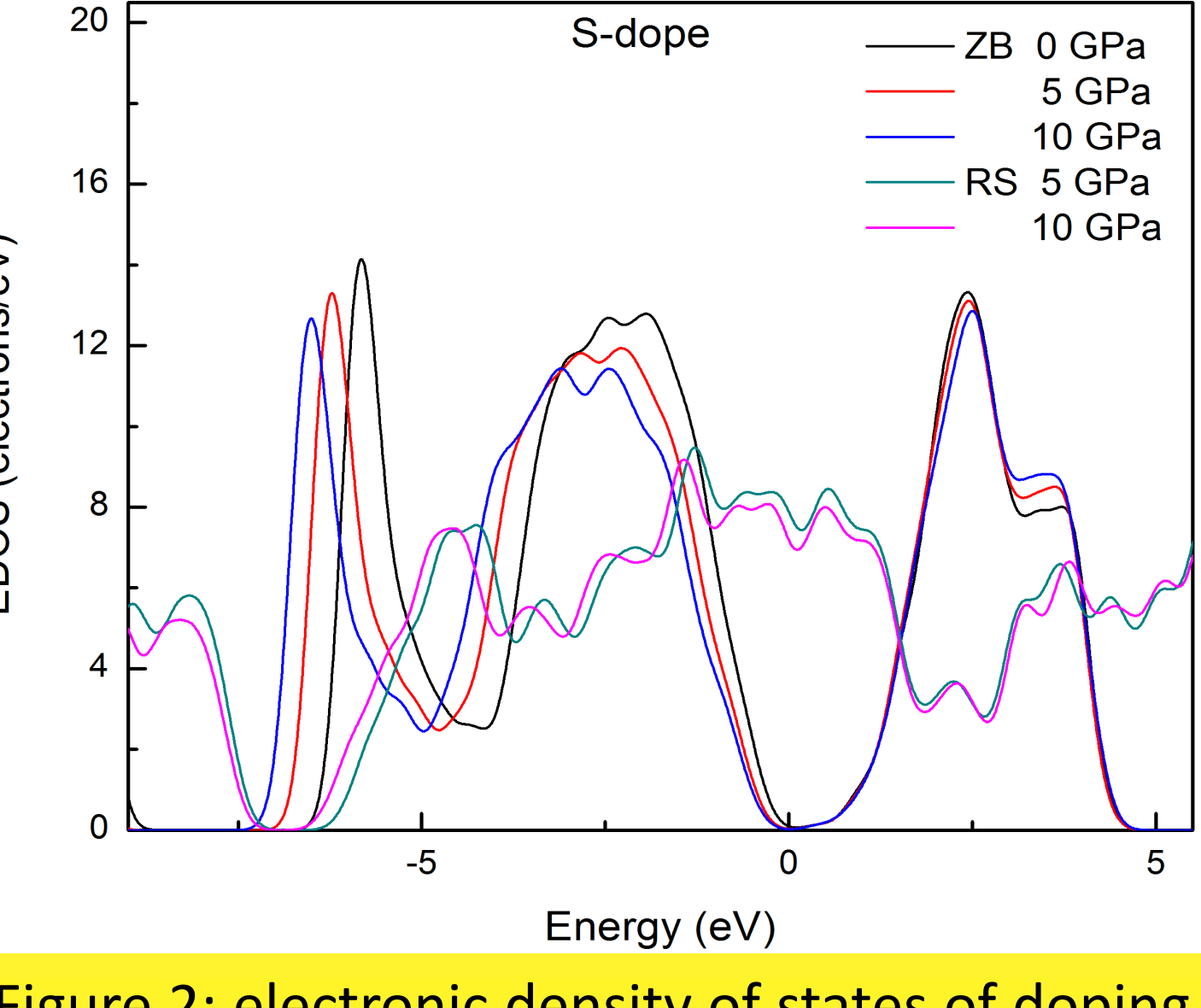


Figure 2: electronic density of states of doping InP under pressure.

Table 3: Comparisons of elastic parameters of InP at ambient pressure.

Р	functional	<b>c</b> <sub>11</sub>	<b>c</b> <sub>12</sub>	C <sub>44</sub>	В	G	Y	e
0	LDA	100.6	55.9	46.2	70.8	34.5	60.7	0.357
	PBE	86.8	45.5	42.0	59.3	31.5	55.6	0.344
	PBEsol	93.4	51.6	43.1	65.5	32.2	56.6	0.356
	Exp. [3]	101	56	45	71	22.5	61	0.360

Table 4: Elastic parameters of In(P,S) under pressure.

S-doped	P(GPa)	<b>c</b> <sub>11</sub>	C <sub>12</sub>	C <sub>44</sub>	В	G	Υ	e
ZB	0	86.7	51.6	32.8	63.3	25.5	48.2	0.371
	5	106.3	75.9	30.4	86.1	23.0	43.1	0.416
	10	124.3	99.3	28.7	107.6	20.6	36.2	0.444
RS	10	251.2	74.1	30.0	133.1	47.1	217.5	0.228

We compare the elastic parameters in the ZB phase (0 GPa), which obtained from varying the density functionals, shown in table 3. All of the elastic constants calculated from DFT with LDA functional satisfy the Born stability criteria that is the requirements for mechanical stability. LDA gave a good results, when compare with experiment. In figure 4, S-doped on P site reduces elastic constants of InP, but it increases under high-pressure.  $c_{11}$ , G and Y in RS phase are higher than in ZB phase. Bulk modulus and ductility of InP are increased by adding S atom and pressure.

### References

- [1] M.C. Payne, M.P. Teter, D.C. Allan, T.A. Arias, D. Joannopoulos, *Rev. Mod. Phys.* 64 (1992): 1045.
- [2] M.D. Segall, P.L.D. Lindan, M.J. Probert, C.J. Pickard, P.J. Hasnip, S.J. Clark, M.C. Payne, *J. Phys.: Cond. Matt.* 14 (2002): 2717.
- [3] D.N. Nichols, D.S. Rimai, R.J. Sladek, Sol. Stat. Comm. 36 (1980): 667.